



1 **Dramatic changes in atmospheric pollution source contributions for a coastal**
2 **megacity in North China from 2011 to 2020**

3

4 Baoshuang Liu^{1,2}, Yanyang Wang^{1,2}, He Meng³, Qili Dai^{1,2}, Liuli Diao^{1,2}, Jianhui
5 Wu^{1,2}, Laiyuan Shi³, Jing Wang³, Yufen Zhang^{1,2*}, and Yinchang Feng^{1,2*}

6

7 ¹State Environmental Protection Key Laboratory of Urban Ambient Air Particulate
8 Matter Pollution Prevention and Control & Tianjin Key Laboratory of Urban
9 Transport Emission Research, College of Environmental Science and Engineering,
10 Nankai University, Tianjin, 300350, China

11 ²CMA-NKU Cooperative Laboratory for Atmospheric Environment-Health Research,
12 Tianjin 300350, China

13 ³Qingdao Eco-environment Monitoring Center of Shandong Province, Qingdao,
14 266003, China

15

16

17 *Correspondence to:* Y.F. Zhang (zhafox@nankai.edu.cn) and Y.C. Feng
18 (fengyc@nankai.edu.cn)



19 Abstract

20 Understanding the effectiveness of long-term air pollution regulatory measures is
21 important for control policy formulation. Efforts have been made using chemical
22 transport modelling and statistical approaches to evaluate the efficacy of the Clean Air
23 Action Plan (2013-2017, CAAP) and the Blue Sky Protection Campaign (2018-2020,
24 BSPP) enacted in China. Changes in air quality due to reduction in emissions can be
25 masked by meteorology, making it highly challenging to reveal the real effects of
26 control measures. Knowledge gap still existed with respect to how sources changed
27 before and after the CAAP and BSPP implemented, respectively, particularly in
28 coastal area where anthropogenic emissions mixed with additional natural sources
29 (e.g., marine aerosol). This work applied a machine learning-based meteorological
30 normalization approach to decouple the meteorological effects from air quality trend
31 in a coastal city in northern China (Qingdao). Secondly, the relative changes in source
32 contributions to ambient $PM_{2.5}$ with a ~10-year observation interval (2011-2012, 2016,
33 and 2019) were also investigated. We discovered that the largest emission reduction
34 section was likely from coal combustions, as the meteorologically normalized SO_2
35 dropped by ~15.5% per year and dispersion normalized SO_4^{2-} decreased by ~41.5%
36 for annual average. Change in the meteorologically normalized NO_2 was relatively
37 stable (~1.0% yr^{-1}), and NO_3^- changed inappreciable in 2016-2019 but significantly
38 higher than that prior to the CAAP. Crustal dust decreased remarkably after the CAAP
39 began. Industrial emissions, for example, steel-related smelting, decreased after 2016
40 due to the relocation of steelmaking enterprises. Note that vehicle emissions were
41 increased in importance, as opposed to the other primary sources. Similar to other
42 mega cities, Qingdao also risks increased ozone pollution that in turns facilitate
43 secondary particles formation in the future. The policy assessment approaches applied
44 in this work also work for other places where air quality management is highly in
45 demand to reduce air pollution.

46
47 **Key words:** Air quality; Random forest; Dispersion normalization; Source
48 apportionment; Coastal megacity



50 **1 Introduction**

51 Rapid industrial development and energy consumption in China over the past several
52 decades have resulted in severe air pollution (Dai et al., 2021; Huang et al., 2014; Zhang et al.,
53 2012). Fine particulate matter (PM_{2.5}, particles with aerodynamic diameter $\leq 2.5 \mu\text{m}$) is the
54 leading health-risk factor for attributable mortality in China (Cohen et al., 2017). It is well-
55 documented that exposure to PM_{2.5} has been associated with increased mortality (Liu et al.,
56 2021b; Joshi et al., 2021; Vodonos and Schwartz, 2021). The world health organization
57 (WHO) recently set the annual average concentration of PM_{2.5} to $5 \mu\text{g m}^{-3}$. Most countries or
58 regions are facing great challenge now to meet the guideline since their current PM_{2.5} levels
59 are well above the latest threshold.

60 To alleviate the severe impact of air pollution on the living environment and public
61 health, the State Council of China released a five-year “Air Pollution Prevention and Control
62 Action Plan” in 2013 (hereinafter the “Clear Air Action Plan, CAAP”)
63 (http://www.gov.cn/zwggk/2013-09/12/content_2486773.htm, last access: 29 October 2021).
64 This was followed by the tighter “Three-year Action Plan to the Blue Sky Protection
65 Campaign” (hereinafter the “Blue Sky Protection Campaign, BSPPC”) in 2018
66 (http://www.gov.cn/zhengce/content/2018-07/03/content_5303158.htm, last access: 29
67 October 2021). The executions of these measures significantly improved air quality (Jiang et
68 al., 2021), thus gained appreciable health benefits (Huang et al., 2018). Vu et al. (2019)
69 demonstrated that the control measures requested by the CAAP have tremendously reduced
70 the emissions (after meteorologically normalized pollutants) in PM_{2.5}, PM₁₀, NO₂, SO₂, and
71 CO in Beijing from 2013 to 2017 by approximately 34%, 24%, 17%, 68%, and 33%,
72 respectively. Xu et al. (2021) found that by 2020, PM_{2.5} reduction measures avoided 3561
73 thousand morbidity cases and 24 thousand premature deaths in the Beijing-Tianjin-Hebei
74 region.

75 Evaluation of the effectiveness of air pollution controls is important for control policy
76 formulation to further improve future air quality (Dai et al., 2020). Many studies have been
77 carried out to evaluate the efficacy of control measures around the world. For example,
78 assessments on short-term control measures were made for the 2008 Olympic Games
79 (Schleicher et al., 2012), 2013 Second Asian Youth Games in Nanjing (Qi et al., 2016), 2014



80 Asia Pacific Economic Cooperation (Xu et al., 2019b), 2015 Military Parade (Wang et al.,
81 2017), and 2017 Belt and Road Forum for International Cooperation (Ma et al., 2020), as
82 well as the 2020 COVID-19 worldwide lockdown (Beloconi et al., 2021; Chen et al., 2020a;
83 Cucciniello et al., 2022; Shi et al., 2021; Wang et al., 2021a). Medium-term (3–5 years)
84 evaluations on the validity of control measures have also been examined (Li et al., 2021b; Yu
85 et al., 2019; Zhang et al., 2019). In contrast, long-term (~10 years) evaluations on controls
86 were rarely reported (Masiol et al., 2019). The majority of such studies have focused
87 primarily on the changes in concentrations of criterion air pollutants to qualitatively deduce
88 the efficacy of source control (Cheng et al., 2019; Lyu et al., 2017; Li et al., 2020; Wang et al.,
89 2014). For example, Vu et al. (2019) and Liang et al. (2016) applied random forest and non-
90 parametric methods to normalize the impact of meteorological factors to evaluate the changes
91 in air pollutant concentrations and the effect of control measures in Beijing and other cities in
92 China over recent time periods. However, quantitative evaluations of source emissions have
93 not been common (Gulia et al., 2018), due to the lack of long-term particle composition
94 monitoring (Hopke et al., 2020) and only a handful of studies quantitatively assessing source
95 contributions smoothed the disturbance of weather conditions.

96 Qingdao, as an economically developed coastal megacity in northern China, has suffered
97 severe air pollution (Bie et al., 2021; Gao et al., 2020; Li et al., 2017). It has been reported
98 by Li et al. (2021a) that meteorology plays a critical role in the formation of pollution for this
99 coastal region. In addition, based on measures taken in accordance with the “CAAP” since
100 2013 and the “BSPC” since 2018, source interventions such as the relocation and
101 transformation of businesses and industries from the Old Town to port regions (Liu et al.,
102 2021a) have been implemented to improve the air quality in Qingdao. Up to now, the air
103 quality in Qingdao has been greatly improved. However, there is no report to date has
104 evaluated the effectiveness of these control measures based on a long-term time scale after
105 these control measures were put into practice, especially for quantitating the changes in
106 source contributions by smoothing the influences of weather conditions. In view of this, our
107 work was mainly to evaluate the implementation of control measures utilizing the data of
108 weather-normalized air pollutants, changes in chemical compositions in PM_{2.5} and source
109 contributions as well as extra source origins from 2011 to 2020. Findings of this work are



110 expected to provide the basis for policy development for a coastal megacity in the future.

111

112 **2 Materials and methods**

113 **2.1 Study region and sampling site**

114 Qingdao is an economically developed coastal megacity of Shandong province, China
115 (Fig. S1). The variation of local economic and social developments from 2011 to 2019 were
116 counted and are shown in Fig. S2. During this period, the local resident population continued
117 to rise, reaching 9499.8 thousand in 2019. The developed area and the possession of civil
118 motor vehicles also showed upward tendency, attaining 758.2 km² and 3062 thousand units in
119 2019, respectively. The total energy consumption had a maximum of 16891 thousand tons
120 standard coal in 2012 and maintained comparable levels from 2014 to 2019. The industrial
121 coal burning capacity above the designated scale and the volume of liquefied petroleum
122 supply both presented downward trend with values of 10965.7 and 30.2 thousand tons in
123 2019, respectively. The emissions of sulfur dioxide, nitrogen oxide, and dust basically
124 showed a downward trend from 2011 to 2019, especially in 2017, and the emissions of these
125 pollutants remained at relatively low levels after 2017, reflecting that the pollution sources
126 for these particular contaminants had been effectively controlled in Qingdao.

127 In this study, in order to evaluate the effectiveness of control measures targeted for
128 polluted sources in the past decade in Qingdao, ambient PM_{2.5} samples were collected at
129 urban sites over three time periods during 2011–2012, 2016, and 2019. The 2011–2012
130 samples were collected before the “CAAP” was enacted in 2013, and the 2016 samples were
131 collected at the end of the “CAAP”, while the 2019 samples were collected during the
132 middle of the “BSPC” policy period. The sampling plan (detailed in the next section) was
133 designed to capture changes in the data during these periods, as any changes could reflect
134 changes in the pollution sources during different stages of China's air pollution control
135 measures. The sites of Licang and Shinan were sampled in 2011–2012, while five additional
136 sites, Shibei, Laoshan, Chengyang, Huangdao, and Jiaonan were sampled in 2016 and 2019
137 (Fig. S1). All collection sites were situated on building rooftops ~10–15 m above ground
138 level and used to collect ambient PM_{2.5} samples. Further descriptions of the seven sampling
139 sites are shown in Table S1.



140 2.2 Sampling and analysis

141 The sampling periods covered all seasons per year and lasted 41, 56, and 64 days for
142 2011-2012, 2016, and 2019, respectively (Table S2). Particles were gathered simultaneously
143 to polypropylene filters and quartz filters loaded to sampling instruments. The details of the
144 sampling instruments and filters in the different years are listed in Table S3. Samples were
145 collected for a duration of 22 h from 11:00 to 09:00 of the next day. Field blanks and parallel
146 samples were synchronously collected at each site. Before sampling, to remove some volatile
147 compounds and impurities, the quartz and polypropylene filters were baked in an oven at 500
148 °C and 60 °C for 2 h, respectively. After sampling, all the filters were stored at 4 °C before
149 gravimetric and chemical analyses were conducted.

150 Before gravimetric analysis, filter equilibration for 48 h was needed under a constant
151 temperature (20 ± 1 °C) and humidity (45–55%). All filters were weighed by the
152 microbalances with a resolution of 1 or 10 µg during different sampling periods; detailed
153 information is listed in Table S4. To ensure the accuracy, static was eliminated before
154 weighting and all filters were weighed at least twice to meet error requirements (Table S4).
155 For chemical analysis, the elements of Na, Mg, Al, Si, K, Ca, Ti, V, Mn, Fe, Ni, Cu, Zn, and
156 Pb were analyzed in different years. For samples collected in 2011-2012 and 2016,
157 inductively coupled plasma-mass spectrometer (ICP-MS) was applied to determine these
158 elements. For samples collected in 2019, inductively coupled plasma-optical emission
159 spectrometer (ICP-OES) was used to measure all related elements. Water-soluble inorganic
160 ions of NO_3^- , SO_4^{2-} , NH_4^+ , and Cl^- were determined using the ion chromatographs during
161 different years. The organic carbon (OC) and elemental carbon (EC) of samples during
162 different years were determined using a thermal/optical carbon analyzer, based on the
163 IMPROVE (in 2011-2012) and IMPROVE_A (in 2016 and 2019) thermal/optical reflectance
164 protocol. The detailed instrumental information is listed in Table S5 and analysis procedures
165 and quality controls are described in Text S1 in the supplemental materials as well as prior
166 works from Liu et al., (2021a), Huang et al. (2021), Wang et al. (2021b), and Tian et al.,
167 (2014).

168 2.3 Random forest (RF) based weather normalization

169 From 1 January 2015 to 31 December 2020, the hourly concentrations of six air



pollutants ($\text{PM}_{2.5}$, PM_{10} , SO_2 , NO_2 , CO , and O_3) at the nine national air quality monitoring stations in Qingdao were collected from the China National Environmental Monitoring Network (CNEM) (<http://106.37.208.233:20035>, last access: 29 October 2021). Data collected from the nine monitoring stations were averaged to represent the pollution level at city scale. The explanatory variables including the meteorological variables and time variables were used to build the RF model and predict the air pollutant concentrations. Hourly surface meteorological data including wind speed, wind direction, temperature, dewpoint, relative humidity, and pressure recorded at Qingdao Liuting International Airport were downloaded using the “worldMet” R package (Carslaw, 2017). Time variables included Unix time (number of seconds since 1 January 1970), Gregorian day (day of the year), month, week, weekday, and hour of the day. Data were analyzed in RStudio with a series of packages, and the details of the random forest (RF) model and weather normalization using the RF model are provided in Vu et al. (2019). The training data set was comprised of 80% of the whole data, with the rest as testing data. After the RF predictive model was built for every pollutant, the model was then fed with a new dataset comprised of time variables same with the original dataset and meteorological variables that resampled from the whole observation. The prediction process was repeated 500 times to predict the concentration of a pollutant. The 500 predicted concentrations were then averaged to calculate the weather normalized concentration. The RF based weather normalization technique has been extensively used to decouple meteorology from the observed concentrations, thus can detect interventions in emissions over time (Dai et al., 2020; Grange et al., 2018, 2019).

192

193 2.4 Theil-Sen regression

The Theil-Sen regression technique has been commonly used to explore the long-term trend of pollutants over years. This approach assumes monotonic linear trends (Masiol et al., 2019). Its principle is to calculate the slopes of all possible pairs of pollutant concentrations, select the median value, and give accurate confidence intervals (Munir et al., 2013; Sen, 1968). In this study, the data of air pollutants obtained from RF modelling with weather normalization was de-seasonalized as the Theil-Sen regression being performed. The Theil-



200 Sen function is provided by the “openair” R package.

201 2.5 Dispersion normalization

202 The concentrations of ambient particles are affected by both local emissions and
 203 meteorological dispersion (Sujatha et al., 2016). Dispersion normalization helps stabilize the
 204 variation of concentrations due to atmospheric dispersion (Sofowote et al., 2021); therefore,
 205 in this study, the contributions of local emissions to particle concentrations were highlighted.
 206 Research suggests that the quantities for particles dispersion can be determined by the
 207 ventilation coefficient (VC) (Kleinman et al., 1976; Iyer and Raj, 2013), which is defined as
 208 the multiplication of mixed layer height (MLH) and the mean wind speed (WS) within the
 209 mixed layer (Eq. (1)). Basing on a VC at a given time interval i , the normalized concentration
 210 can be obtained by Eq. (2):

$$211 \quad VC_i = MLH_i \times WS_i \quad (1)$$

$$212 \quad C_{vc,i} = C_i \times \frac{VC_i}{VC_{mean}} \quad (2)$$

213 where VC_i ($\text{m}^2 \text{s}^{-1}$) is the ventilation coefficient during period i , VC_{mean} ($\text{m}^2 \text{s}^{-1}$) is the mean
 214 VC during the whole study period, and $C_{vc,i}$ ($\mu\text{g m}^{-3}$) and C_i ($\mu\text{g m}^{-3}$) are the normalized and
 215 observed concentrations, respectively. In this study, the dispersion normalization was
 216 conducted for ambient $\text{PM}_{2.5}$ and chemical compositions and the resolved source
 217 contributions. The surface wind speed at 10 m was replaced with the mean wind speed
 218 through MLH because of the absence of wind speed at different heights (Dai et al., 2020;
 219 Ding et al., 2021). The 3 h resolution data of MLH and WS was derived from archived
 220 meteorology of the National Ocean and Atmospheric Administration
 221 (<https://www.ready.noaa.gov/READYamet.php>, last access: 29 October 2021), and the
 222 calculated daily MLH and WS data were used in this study.

223 2.6 Positive matrix factorization (PMF)

224 In order to assess the effectiveness of pollution control, source categories and their
 225 contribution were estimated by the PMF method. The PMF decomposes a sample
 226 composition dataset (X) into two matrices including source profiles (F) and source
 227 contributions (G) (Paatero and Tapper, 1994). This principle can be refined as follows:

$$228 \quad x_{ij} = \sum_{k=1}^p g_{ik} f_{kj} + e_{ij} \quad (3)$$



where x_{ij} is the concentration ($\mu\text{g m}^{-3}$) of the j th component from the i th sample; g_{ik} means the contribution ($\mu\text{g m}^{-3}$) of the k th source to the i th sample; f_{kj} represents the source profile ($\mu\text{g m}^{-3}$) of the j th component from the k th source; e_{ij} is the residual ($\mu\text{g m}^{-3}$) of the j th component of the i th sample; and p means the number of sources. In this study, US EPA PMF v5.0 was applied to carry out source apportionment, and the details in treatment of input data and method detection limits of chemical compositions are described in Table S6 and Text S2, respectively.

2.7 Potential source contribution function (PSCF)

We performed PSCF to further investigate the origin of polluted source. First, the 72 h backward trajectories were calculated at 6 h intervals every day with starting height of 100m above ground level in Qingdao (36.10° N , 120.32° E), using the Hybrid Single-Particle Lagrangian Integrated Trajectory (HYSPLIT) model in the GIS-based software of TrajStat (Liu et al., 2020). The weather data was acquired from Global Data Assimilation System with horizontal resolution of one-degree latitude-longitude (available at <http://www.arl.noaa.gov/>, last access: 29 October 2021). PSCF was then analyzed based on the trajectories added to source concentrations. The study region was divided into equal-sized grid cells, thus the number of endpoints for given specific values in every cell could be obtained. According to pre-set threshold criterion, the PSCF value was the proportion of the number of endpoints beyond the threshold criterion in each cell. To improve the accuracy of the result, weighted PSCF was calculated. More details are given in Text S3 of supplementary material.

3 Results and discussion

3.1 Variation characteristics of the air quality

3.1.1 Trend analysis and annual changes

The annual mean concentration of $\text{PM}_{2.5}$ and PM_{10} in Qingdao decreased by 38% and 38% from 51 and $98\ \mu\text{g m}^{-3}$ in 2015 to 32 and $61\ \mu\text{g m}^{-3}$ in 2020, respectively. The annual mean $\text{PM}_{2.5}/\text{PM}_{10}$ was 0.47 ± 0.02 , with little change from 2015 to 2020, suggesting the significant impact of coarse particle sources (e.g. dust) in Qingdao. The annual mean levels of SO_2 and NO_2 declined by 72% and 8% from 27 and $33\ \mu\text{g m}^{-3}$ in 2015 to 8 and $31\ \mu\text{g m}^{-3}$ in 2020, respectively. The concentration of SO_2 showed a significant downward trend, while



259 that of NO_2 changed little, probably indicating that the impact of coal-fired sources was
260 significantly reduced, while the impact of mobile sources might still be obvious. The annual
261 mean level of CO decreased by 32% from 0.91 mg m^{-3} in 2015 to 0.62 mg m^{-3} in 2020, while
262 that of O_3 changed little with ranging from 71 to $69 \mu\text{g m}^{-3}$.

263 In order to shield the impact of meteorological dispersion, the normalized air quality
264 parameters were acquired using the RF algorithm under 30-year average (1990–2020)
265 meteorological conditions. The Theil–Sen trends of air pollutant concentrations after weather
266 normalization by RF modelling are shown in Fig. 1. The decreasing real trend for air
267 pollutants except for O_3 was found after the weather normalization (Fig. 1), indicating that
268 the air quality is gradually improving in Qingdao. The trends of the normalized air quality
269 parameters represent the effects of emission control and, in some cases, associated chemical
270 processes (Vu et al., 2019). The Theil–Sen trend analysis of air pollutant concentrations and
271 $\text{PM}_{2.5}/\text{PM}_{10}$ and SO_2/NO_2 after the weather normalization is shown in Fig. 1. Compared with
272 other air pollutants, the decline rate of SO_2 concentration was the highest (a median of 15.5%
273 yr^{-1}), whereas that of O_3 concentration was the lowest ($0.2\% \text{ yr}^{-1}$). Note that the decline rate
274 of $\text{PM}_{2.5}$ concentration ($6.0\% \text{ yr}^{-1}$) was higher than that of PM_{10} concentration ($5.6\% \text{ yr}^{-1}$),
275 which led to a slight downward trend for $\text{PM}_{2.5}/\text{PM}_{10}$ ($0.6\% \text{ yr}^{-1}$), indicating that the impact
276 of coarse particle sources such as dust might be prominent. The decline rate of SO_2
277 concentration was higher than that of NO_2 concentration ($1.0\% \text{ yr}^{-1}$), resulting in a higher
278 SO_2/NO_2 decline rate of $15.3\% \text{ yr}^{-1}$, indicating that the control effect of stationary sources
279 was better than that of mobile sources (Nirel and Dayan, 2001). It was found that CO
280 concentration also performed an obvious decreasing trend, with the decreasing rate reaching
281 $5.2\% \text{ yr}^{-1}$, whereas the downward trend of O_3 concentration was not prominent. The
282 normalized medians of $\text{PM}_{2.5}$, PM_{10} , SO_2 , NO_2 , CO and O_3 decreased by 2.8, 5.4, 3.4, 0.3,
283 42.8, and $0.1 \mu\text{g m}^{-3} \text{ yr}^{-1}$, respectively (Table S7).

284 Figure S3 compares the trends of air pollutants before and after normalization from 2015
285 to 2020, which are largely different depending on meteorological conditions (Vu et al., 2019).
286 The annual average concentrations of $\text{PM}_{2.5}$, PM_{10} , SO_2 , NO_2 , CO, and O_3 after normalization
287 were higher than the actual observed concentrations. Compared with 2018, the observed
288 concentrations of air pollutants in 2019 showed an increase in varying degrees; however, the



289 increasing values of annual average concentrations for PM_{2.5}, PM₁₀, SO₂, CO, and O₃ after
 290 normalization decreased, and even the NO₂ concentration after normalization also decreased.
 291 This indicates that the meteorological conditions in 2019 reduced the effect of actual control
 292 to some extent. Up to that point, emission control had resulted in reductions of PM_{2.5}, PM₁₀,
 293 SO₂, NO₂, CO, and O₃ concentrations by 17.7%, 31.9%, 18.4%, 1.7%, 0.3%, and 0.4% from
 294 2015 to 2020, respectively, highlighting that much work is still needed to ensure the decrease
 295 of NO₂ and O₃ concentrations in the future.

296

297 3.1.2 Changes in the air quality in the two control stages

298 In order to assess the changes in ambient air quality in Qingdao during different policy
 299 control periods, this study analyzed the changes in air pollutant concentrations during two
 300 stages: the CAAP period (stage 1: 2015-2017) and the BSPP period (stage 2: 2018-2020).
 301 The observed annual mean concentrations for PM_{2.5} and PM₁₀ during stage 1 were 45 and 89
 302 $\mu\text{g m}^{-3}$, respectively (Table S8), and their annual average decline rates were 11.9% and 8.0%
 303 after weather normalization, respectively. Compared with stage 1, the annual average
 304 concentrations of PM_{2.5} and PM₁₀ observed in stage 2 were 35 and 71 $\mu\text{g m}^{-3}$, respectively
 305 (Table S8), and the decline range after normalization was reduced, with the decline rates of
 306 5.3% and 7.0%, respectively (Fig. 2). However, PM_{2.5}/PM₁₀ ratios during two stages were
 307 less than 0.5, suggesting that the impact of dust sources might be obvious in the two stages.
 308 Note that the mean observed annual concentration of SO₂ was 21 $\mu\text{g m}^{-3}$ in the stage 1 (Table
 309 S8) and its annual average decline rate reached 25% after normalization (Fig. 2), which was
 310 significantly higher than that of other pollutants. Compared with stage 1, the observed annual
 311 average concentration of SO₂ in stage 2 was only 8 $\mu\text{g m}^{-3}$ (Table S8), and the annual decline
 312 rate of SO₂ concentration after normalization still reached 17.1% (Fig. 2), indicating that
 313 Qingdao had achieved remarkable results in the control of coal combustion during the two
 314 stages. The observed annual mean concentrations for NO₂ and O₃ during stage 1 were 34 and
 315 73 $\mu\text{g m}^{-3}$, respectively (Table S8), and their annual increasing rates after normalization were
 316 1.5% and 2.8%, respectively (Fig. 2). The observed annual mean concentrations of NO₂ and
 317 O₃ in stage 2 were 32 and 71 $\mu\text{g m}^{-3}$, respectively (Table S8), while their annual decline rates
 318 after normalization were only 2.7% and 2.0%, respectively (Fig. 2). This indicates that the



319 impact of motor vehicles in Qingdao could be greater than expected. Meanwhile, NO₂ and
320 volatile organic compounds emitted from motor vehicles are important precursors for the
321 formation of O₃ (Pugliese et al., 2014; Tsai et al., 2010), which were found to have further
322 enhanced the O₃ concentration in Qingdao's atmosphere. The mean observed annual
323 concentrations for CO were 0.80 and 0.64 mg m⁻³ in stages 1 and 2, respectively (Table S8),
324 and the annual average decline rate were 11.4% and 3.2% after normalization, respectively
325 (Fig. 2), suggesting that there might have been a benefit from the significant control effect of
326 coal-fired sources.

327 Diurnal variations of concentrations of air pollutants and PM_{2.5}/PM₁₀ and SO₂/NO₂
328 after normalization in the two stages are shown in Fig. S4. The diurnal variation in PM_{2.5}
329 concentration in the two stages was basically the same; however, the concentration of PM_{2.5}
330 in stage 2 was significantly lower than that in stage 1. Diurnal variation of PM₁₀
331 concentration in the two stages was similar to PM_{2.5}. The daily variations of PM_{2.5}/PM₁₀ in
332 the two stages were basically the same, and the PM_{2.5}/PM₁₀ between 06:00-20:00 in stage 2
333 was slightly lower than that in stage 1, probably suggesting that the impact of dust increased
334 slightly during this period. The diurnal variations of SO₂ and CO concentrations during
335 stages 1 and 2 were generally consistent, whereas their concentrations in stage 2 were
336 substantially lower than those in stage 1, which might indicate that the control effects of coal
337 combustion in Qingdao in stage 2 was obvious. In contrast, the diurnal variations of NO₂
338 concentrations in stages 1 and 2 were basically consistent with the values at each time,
339 suggesting that the impact of motor vehicles in Qingdao might still be significant, especially
340 the morning and evening peaks and between 21:00 and 23:00 at night. The daily variations of
341 O₃ concentrations were highly consistent in the two stages, especially between 14:00 and
342 17:00, O₃ pollution was still severe. In general, compared with stage 1, the concentrations of
343 PM_{2.5}, PM₁₀, SO₂, and CO in stage 2 decreased remarkably at all times, while those of NO₂
344 and O₃ remained basically unchanged at all times, indicating that the control effect of coal-
345 fired sources in Qingdao was significant, whereas the impact of motor vehicles and O₃
346 pollution were more obvious.
347



348 3.1.3 Changes in air quality after the COVID-19 lockdown

349 In response to the COVID-19 outbreak, a series of lockdown measures were
350 implemented in China to curb the virus transmission, resulting in a significant decrease in
351 traffic and industrial activities. These limitations provided an opportunity to investigate
352 critical pollution sources that could potentially be better managed in the future to further
353 improve the air quality. In order to explore the changes of air quality in Qingdao during the
354 COVID-19 lockdown period, combined with the specific lockdown situation of Qingdao
355 (http://wsjkw.shandong.gov.cn/ywdt/xwtt/202001/t20200124_3420319.html;
356 http://www.shandong.gov.cn/art/2020/3/7/art_119816_350607.html; last access: 29 October
357 2021), this study divided the lockdown period into three stages: pre-lockdown (1 to 24
358 January, 2020), full lockdown (25 January to 7 March, 2020), and partial lockdown (8 to 31
359 March, 2020). The time series and average values of air pollutant concentrations and
360 $\text{PM}_{2.5}/\text{PM}_{10}$ and SO_2/NO_2 during different lockdown stages and their corresponding periods
361 in 2018 and 2019 are shown in Fig. 3 and Tables S9-S10. According to the weather
362 normalization data, compared with that before the lockdown, the concentrations of $\text{PM}_{2.5}$,
363 PM_{10} , SO_2 , NO_2 , and CO decreased substantially during the full lockdown, among which the
364 concentrations of PM_{10} and NO_2 decreased the most (49.5% and 49.0%, respectively),
365 followed by $\text{PM}_{2.5}$ (47.8%) (Table S11), which was closely related to the significant decrease
366 in traffic and construction activities during the full lockdown (Collivignarelli et al. 2021;
367 Hong et al. 2021; Wang et al. 2021a). Note that the O_3 concentration increased apparently by
368 50.8% during the full lockdown (Table S11), suggesting that the atmospheric oxidation might
369 be enhanced during this period, similar to the study of Chu et al. (2021), Ding et al., (2021),
370 He et al., (2020), and Le et al. (2020). PM_{10} and NO_2 concentrations rebounded significantly
371 during partial lockdown, increasing by 20.3% and 21.1% compared with the full lockdown,
372 respectively, likely due to the increased impacts of traffic activities and related road dust. The
373 concentrations of $\text{PM}_{2.5}$, SO_2 , and CO further decreased during the partial lockdown. The
374 study from Yin et al. (2021) showed that the decrease of $\text{PM}_{2.5}$ concentration might be mainly
375 due to the meteorological conditions.

376 Compared with the same period in 2018, the concentrations of $\text{PM}_{2.5}$, PM_{10} , SO_2 , NO_2 ,
377 CO, and O_3 decreased obviously during the full lockdown, of which the reduction range of



SO₂ concentration was the greatest (39.8%), whereas that of O₃ concentration was relatively lowest (1.8%) (Table S12). Compared with the corresponding period in 2019, the concentrations of PM_{2.5}, PM₁₀, SO₂, NO₂, and CO decreased by 34.5%, 44.8%, 27.0%, 32.6%, and 22.3% during the full lockdown, respectively, while that of O₃ increased by 3.9% (Table S12). This shows that the COVID-19 lockdown measures led to the marked decrease of the primary emissions of air pollutants. Meanwhile, the concentrations of particulate matter and NO₂ decreased substantially during the full lockdown. Since there are relatively few industrial enterprises in urban area of Qingdao, NO₂ is mainly emitted from motor-vehicles. Therefore, this suggested that the control of motor-vehicles under normal conditions should play an important role in the improvement of air quality in Qingdao.

3.2 Changes in meteorological conditions and chemical compositions

In this study, the ventilation coefficient in the same period was used to normalize the concentrations of chemical compositions in PM_{2.5}. After reducing the impacts of meteorological dispersion, the changes in the concentrations of major chemical compositions in the different years were analyzed to better reflect the impacts of source emissions (Dai et al., 2020; Ding et al., 2021). In 2011-2012, 2016, and 2019, the annual average MLHs in Qingdao were 399, 383, and 414 m, respectively (Fig. S5). However, the average wind speed in 2016 was significantly higher than that in other years, reaching 3.3 m s⁻¹. The ventilation coefficient showed an increasing trend year by year, from 1292.7 to 1555.4 m s⁻² (Fig. S5), suggesting that the atmospheric dispersion conditions in Qingdao were gradually increasing. The average ventilation coefficient of Qingdao in three years was 1432.6 m s⁻², and higher MLH usual corresponds to higher wind speed. Time series of observed concentrations and normalized concentrations of PM_{2.5} and chemical compositions are shown in Fig. S6. The observed and normalized concentrations of PM_{2.5} during the whole study period were 93 and 83 μg m⁻³, suggesting that unfavorable meteorological conditions generated approximately 10 μg m⁻³ of growth of PM_{2.5}, which was significantly lower than that reported by the study of Ding et al. (2021) during the COVID-19 lockdown in Tianjin.

The annual changes in the observed and dispersion normalized concentrations and percentages of main chemical compositions in ambient PM_{2.5} are shown in Fig. 4 and Fig. S7.



408 From 2011-2012 to 2019, the observed concentrations of SO_4^{2-} showed an obvious downward
409 trend, from 23.5 to 6.7 $\mu\text{g m}^{-3}$. The trend of concentrations of SO_4^{2-} after dispersion
410 normalization was consistent with the observed concentrations, and the annual average
411 decline rate was approximately 41.5% (38.1% in 2016 and 44.8% in 2019) (Table S13),
412 probably suggesting that the impacts of coal-fired sources in Qingdao has decreased
413 substantially in recent years. In contrast, the observed concentrations and percentages of NO_3^-
414 increased significantly from 2011-2012 (3.5 $\mu\text{g m}^{-3}$) to 2019 (10.0 $\mu\text{g m}^{-3}$), and $\text{NO}_3^-/\text{SO}_4^{2-}$
415 increased from 0.14 to 1.50. After dispersion normalization, the concentrations and
416 percentages of NO_3^- changed inappreciable in 2016-2019 but significantly higher than that
417 prior to the CAAP. It has been found that ambient NO_3^- in urban mainly originates from the
418 secondary conversion of NO_x emitted by motor-vehicles (Alexander et al., 2020; Liu et al.,
419 2017; Meng et al., 2008), thereby indicating that the impacts of motor-vehicles in Qingdao
420 might become increasingly obvious. The observed and normalized concentrations and
421 percentages of OC and EC basically performed a downward trend from 2011 to 2019. The
422 OC concentration decreased significantly, and the observed and normalized concentrations
423 decreased from 13.1 to 7.6 $\mu\text{g m}^{-3}$ and 12.9 to 7.2 $\mu\text{g m}^{-3}$, respectively, which might be related
424 to the significant decrease in the impacts of coal-fired sources in Qingdao. Note that the
425 annual variations of observed and normalized concentrations of NH_4^+ were consistent with
426 that of SO_4^{2-} , but contrary to that of NO_3^- , which might indicate that ammonium mainly
427 existed in the form of ammonium sulfate and ammonia hydrogen sulfate in Qingdao.

428 Crustal elements (Si, Al, and Mg) decreased remarkably after the CAAP were in place.
429 The observed and normalized concentrations of these elements in 2011-2012 were higher
430 than those in 2016 and 2019, while their concentrations in 2019 were slightly higher than
431 those in 2016. From 2011-2012 to 2019, the observed concentrations of Si, Al, and Mg
432 decreased from 10.7 to 1.0 $\mu\text{g m}^{-3}$, 3.1 to 0.5 $\mu\text{g m}^{-3}$, and 1.9 to 0.2 $\mu\text{g m}^{-3}$, respectively, and
433 the trends of normalized concentrations were consistent with the observed concentrations,
434 likely suggesting that the impact of dust in 2011-2012 was apparently higher than that in
435 2016 and 2019, and 2019 rebounded compared with 2016. The trends of the observed and
436 normalized concentrations and percentages of Ca were consistent. The concentrations and
437 percentages in 2011-2012 were remarkably higher than that in 2016 and 2019, and the



concentration in 2019 rebounds compared with that in 2016, with the increasing rate of 77.1% in terms of normalized data (Table S13). This suggests that the impact of construction activities in 2011-2012 might have been significantly higher than that in 2016 or 2019. The annual trends of observed and normalized concentrations of Fe were also consistent. The observed and normalized concentrations in 2011-2012 were 4.0 and $4.6 \mu\text{g m}^{-3}$, respectively. After 2016, the concentrations and percentages of Fe decreased substantially, which might be closely related to the relocation of iron and steel enterprises in Qingdao (Liu et al., 2021a). The observed and normalized concentrations and percentages of Ni and V basically showed a downward trend from 2011-2012 to 2019. The concentrations in 2011-2012 were significantly higher than that in 2016 and 2019, which might indicate that the impact from ships in 2011-2012 was more obvious. Of course, it might also be related to the impact of manual dust sources. From 2011-2012 to 2019, the observed and normalized concentrations and percentages of Na showed a downward trend. The concentration and percentage in 2011-2012 were significantly higher than those in 2016 and 2019, suggesting that the impact of sea salt might have decreased in Qingdao in recent years.

3.3 Changes in source contributions

3.3.1 Source identification

Given that the differences of source profiles during different periods, PMF analysis was conducted for three data sets corresponding to separate sampling periods (i.e., 2011-2012, 2016, and 2019). The solutions from five to nine factors were examined in terms of scaled residuals, factor interpretability, and displacement acceptability (Brown et al., 2015; Dai et al., 2020). An eight-factor solution was chosen as the optimal fits for each data set. The correlation coefficients (R^2) between the observed and calculated concentrations were 0.91, 0.83, and 0.91, respectively (Fig. S8). There were no DISP swaps, and all BS runs had at least 87% agreement with the base case values (Table S14).

The factor profiles estimated from PMF during different periods are shown in Figs. S9-S11. The first factor was identified as vehicle emissions, because OC and EC both had high concentrations and explained variations as well as narrow DISP bounds. It is known that the OC and EC are important tracers for vehicle emissions (Bi et al., 2019; Gao et al., 2016;



468 Ryou et al., 2018; Xu et al., 2019a). The second factor was characterized by higher
469 concentration and explained variation of Si, and high Al concentrations, and they all had
470 narrow DISP ranges. Si and Al were the indicators for fugitive dust (Begum et al., 2011; Jain
471 et al., 2018; Zhao et al., 2021). The third factor featured relatively high concentrations and
472 explained variations of OC, SO_4^{2-} , and Cl^- with tight DISP intervals. These species were
473 distinctive tracers for coal combustion (Huang et al., 2017; Song et al., 2021; Tao et al., 2014).

474 The fourth factor was characterized by high explained variations of Fe and Mn, and
475 relatively high concentrations of Cu and Zn. Tsai et al. (2020) found that Fe and Mn were
476 related to basic oxygen, iron ore sintering and steel oxidation refining. Querol et al. (2007)
477 and Kuo et al. (2007) have reported that Cu and Zn were released from multiple metal
478 smelting. Therefore, this factor was identified as steel-related smelting. The fifth factor was
479 dominated by high concentrations and explained variations of NO_3^- and NH_4^+ with small
480 DISP bounds, which was identified as secondary nitrate (Esmaeilirad et al., 2020). It was
481 found that SO_4^{2-} and NH_4^+ presented the highest explained variations and concentrations with
482 narrow DISP bounds in the sixth factor. Therefore, this factor was assigned as secondary
483 sulphate (Bove et al., 2016; Jain et al., 2020). The seventh factor was featured by high
484 concentration and explained variation of Ca with a small DISP bound, which was identified
485 as construction dust (Zhang et al., 1999; Zhang et al., 2005). The final factor was
486 characterized by highly explained variations of Na, Ni, and V with narrow DISP intervals. In
487 addition, the concentrations of Mg, NO_3^- , SO_4^{2-} , and Cl^- in this factor were also relatively
488 high. Zhang et al. (2021), Liu et al. (2018), Choi et al. (2013), and Police et al. (2016) have
489 found that sea salt involves high amounts of Na, Mg, NO_3^- , SO_4^{2-} , and Cl^- . Meanwhile, Ni
490 and V are the markers of ship emissions (Manousakas et al., 2017; Zong et al., 2018; Xu et al.,
491 2018). Therefore, this factor was recognized as a mixed source of sea salt and ship emissions.

493 3.3.2 Change in source contributions

494 The source apportionment results of ambient $\text{PM}_{2.5}$ in Qingdao from 2011–2012 to
495 2019 are shown in Fig. 5 and Figs. S12–S15. For vehicle emissions, its contribution showed
496 an increasing trend with each year, from $12.1 \mu\text{g m}^{-3}$ (7.9%) to $13.6 \mu\text{g m}^{-3}$ (22.5%). The
497 contribution of coal combustion performed a significant downward trend, from $21.3 \mu\text{g m}^{-3}$



(13.9%) in 2011-2012 to $4.5 \mu\text{g m}^{-3}$ (7.5%) in 2019. The contribution of fugitive dust in 2011-2012 was up to $35.3 \mu\text{g m}^{-3}$ (23.1%), significantly higher than $8.5 \mu\text{g m}^{-3}$ (13.2%) in 2016 and $10.2 \mu\text{g m}^{-3}$ (16.8%) in 2019, and the contribution in 2019 rebounded compared with 2016. The contribution of construction dust showed a downward trend year after year, from $14.2 \mu\text{g m}^{-3}$ (9.3%) in 2011-2012 to $2.4 \mu\text{g m}^{-3}$ (4.0%) in 2019. The contribution of steel-related smelting also showed a downward trend year by year, from $15.9 \mu\text{g m}^{-3}$ (10.4%) in 2011-2012 to $3.0 \mu\text{g m}^{-3}$ (4.9%) in 2019. The significant decline in the impact of steel-related smelting after 2016 might be closely related to the relocation of iron and steel enterprises in Qingdao (Liu et al., 2021a). The contribution of secondary nitrate basically performed a significant upward trend, increasing from $14.5 \mu\text{g m}^{-3}$ (9.5%) in 2011-2012 to $15.2 \mu\text{g m}^{-3}$ (25.2%) in 2019, which might be related to the high concentration of precursor (NO_2) (Fig. 1) and the increase in atmospheric oxidation in recent years (Chen et al., 2020b; Fu et al., 2020). In contrast, the contribution of secondary sulphate showed a significant downward trend, from $34.2 \mu\text{g m}^{-3}$ (22.3%) in 2011-2012 to $9.7 \mu\text{g m}^{-3}$ (16.0%) in 2019, likely due to the significant decrease in the concentration of its precursor (SO_2) (Fig. 1). For sea salt and ship emissions, the contribution basically performed a downward trend, from $5.7 \mu\text{g m}^{-3}$ (3.7%) in 2011-2012 to $2.0 \mu\text{g m}^{-3}$ (3.2%) in 2019.

To shield the impact of meteorology on the source apportionment results, this study used Eq. (2) to conduct the treatment of dispersion normalization for the source apportionment results, and then analyzed the annual changes in the contributions of different source categories, as shown in Fig. S16. The annual changes in the contributions of multiple sources in Qingdao were basically consistent with the results of direct PMF calculation. The contribution of vehicle emissions was increasing year by year, and the annual average increase rate of contribution concentration was 12.1%. However, the contribution of coal combustion showed a continuous yearly downward trend, with the average annual decline rate of contribution concentration being 56.8%. For fugitive dust, compared with 2011-2012, the contribution in 2016 decreased substantially, with a decline rate of contribution concentration of 68.9%, while it rebounded in 2019, with an increase rate of 25.2%. The contribution of construction dust performed a continuous yearly downward trend, with the average annual decline rate of contribution concentration being 55.9%. For the steel-related



528 smelting, and sea salt and ship emissions, the average annual decline rates of their
529 contribution concentrations were 55.3% and 46.0%, respectively. In contrast, the contribution
530 of secondary nitrate showed an increasing trend, and the increase rate of its contribution
531 concentration was 1.7%, while the contribution proportion increased by more than 70%. The
532 contribution of secondary sulphate showed a continuous yearly downward trend, and the
533 average annual decline rate of contribution concentration was 38.7%. Overall, the impacts of
534 coal combustion and steel-related smelting industrial sources in Qingdao decreased
535 substantially over the last decade, suggesting that the controlling effects of these sources were
536 obvious. The impact of motor-vehicles was prominent each year. Qingdao also risks increased
537 emissions from the increased vehicular population and ozone pollution that facilitate
538 secondary particles formation in the future. The impact of fugitive dust had decreased in
539 recent years, whereas its contribution was still obvious. Therefore, the control of motor-
540 vehicles and dust should be the focus of pollution source control in Qingdao in the future,
541 while that of coal combustion and industrial sources also should not be ignored.

542 In this study, the heating season in 2011-2012 was defined from 15 to 29 February,
543 2012, that in 2016 was defined from 17 to 20 December, 2016, and that in 2019 referred from
544 12 to 26 January, 2019. The contributions of different sources during different heating
545 seasons in Qingdao are shown in Figs. S17-S18. Compared with the heating season in 2011-
546 2012, the contribution of coal combustion decreased significantly in the heating seasons of
547 2016 and 2019, from $50.2 \mu\text{g m}^{-3}$ (31.7%) to $10.6\text{-}10.7 \mu\text{g m}^{-3}$ (6.4-10.8%). The contribution
548 percentages after dispersion normalization showed a consistent trend. For vehicle emissions,
549 the contribution percentages in the heating season increased continuously each year, from 3.9%
550 in 2011-2012 to 22.3% in 2019. The results after normalization had the same trend,
551 suggesting that the impact of motor vehicles in heating season was gradually prominent. The
552 contribution of fugitive dust in the heating season in 2011-2012 ($14.2 \mu\text{g m}^{-3}$) was
553 substantially higher than that in 2016 ($3.9 \mu\text{g m}^{-3}$) and 2019 ($12.0 \mu\text{g m}^{-3}$). The contribution in
554 the heating season in 2019 rebounded remarkably compared with that in 2016, and the results
555 of dispersion normalization were consistent. The contribution of construction dust in the
556 heating season in 2019 was markedly lower than that in 2011-2012 and 2016. The
557 contribution of steel-related smelting in the heating season showed a continuous yearly



558 downward trend, from $22.6 \mu\text{g m}^{-3}$ in the heating season from 2011-2012 to $4.6 \mu\text{g m}^{-3}$ in
559 2019. However, its contribution percentage in the heating season in 2019 was higher than that
560 in the heating season in 2016, which was consistent with the normalized results, indicating
561 that the impact of steel-related smelting in the heating season had increased, though the
562 contribution percentage was low. The contribution of secondary nitrate in heating season in
563 2016 was up to $61.3 \mu\text{g m}^{-3}$ (36.3%), which was significantly higher than that of $28.4 \mu\text{g m}^{-3}$
564 (28.9%) in 2019 and $16.8 \mu\text{g m}^{-3}$ (10.6%) in 2011-2012. This was consistent with the results
565 of the dispersion normalization. It can be seen that although the contribution of secondary
566 nitrate in the heating season in 2019 was reduced, its contribution was significantly higher
567 than that of other sources. Similarly, the contribution of secondary sulphate was also higher in
568 the heating season of 2016 than other years; however, its contribution was clearly lower than
569 that of secondary nitrate. After dispersion normalization, the contributions of secondary
570 sulphate basically showed a continuous yearly downward trend. The contribution of sea salt
571 and ship emissions in the heating season also showed an obvious downward trend, from 10.0
572 $\mu\text{g m}^{-3}$ (6.3%) in 2011-2012 to $1.4 \mu\text{g m}^{-3}$ (1.5%) in 2019, and the results after dispersion
573 normalization were basically consistent. The average decline rate of contribution
574 concentration was approximately 70%, including 88% in 2016. From this analysis, the
575 impacts of coal combustion and steel-related smelting in Qingdao were relatively low after
576 the heating season in 2016, while that of vehicle emissions was prominent each year.
577 Although the impact of fugitive dust had rebounded in the heating season in 2019, the
578 contribution was relatively low. The contribution of secondary nitrate in heating season was
579 substantially higher than that of other sources, and the influence of secondary sulfate
580 decreased each year. The influence of sea salt and ship emissions in heating season showed a
581 continuous yearly downward trend.

582

583 3.4 Changes in potential source areas

584 Similar to the studies of Liu et al. (2021a) and Dai et al. (2020), according to the source
585 apportionment results, this study used the PSCF method to analyze the changes in the
586 potential impact areas of emission sources in Qingdao from 2011-2012 to 2019, and the
587 results are shown in Fig. 6. For vehicle emissions, the potential impact areas changed greatly



588 from 2011-2012 to 2019. The potential impact areas in 2011-2012 were located at the
589 junction of Shandong, Henan, Anhui, and Jiangsu provinces, and the potential impact areas
590 were mainly located in the south part of Jiangsu in 2016, while in 2019, Tianjin and the
591 northwest part of Shandong were important impact areas. The potential impact areas for
592 fugitive dust showed a trend of westward migration from 2011-2012 to 2019. For 2011-2012,
593 the potential impact areas were located at the junction of Shandong, Henan, Anhui, and
594 Jiangsu, as well as in the northern part of Shandong. The potential impact areas were located
595 in the northwestern part of Shandong in 2016, while they were at the junction of Shandong
596 and Henan in 2019. For coal combustion, the potential impact areas for 2011-2012 were
597 located at the junction of Shandong, Henan, Anhui, and Jiangsu. In 2016, they moved to the
598 northwest of Shandong Province and Beijing Tianjin and Hebei region, and the northwest of
599 Shandong was an important impact area in 2019. For steel-related smelting, Beijing and
600 Tianjin were the potential impact areas for 2011-2012, while the potential impact area was
601 located in the Yellow Sea in 2016, which might be related to the relocation of iron and steel
602 enterprises to a port area in the south of Qingdao (Liu et al., 2021a). This suggests that the air
603 mass transport in the coastal area could lead the nearby sea areas to become potential impact
604 areas. The potential impact area in 2019 was mainly located at the junction of Hebei, Henan,
605 and Shandong.

606 For secondary nitrate, the potential impact area for 2011-2012 was the junction of
607 Shandong, Henan, Jiangsu, and Anhui provinces. The potential impact area was mainly
608 located in the central and southern parts of Shandong in 2016, while two areas were located
609 in Beijing, Tianjin, and the junction of Hebei, Henan, and Shandong provinces in 2019. For
610 secondary sulphate, the main potential impact areas for 2011-2012 were located at the
611 junction of Shandong, Henan, Jiangsu, and Anhui Provinces and the western part of Jilin
612 Province. The impact of the Middle East of Shandong Province was more obvious in 2016,
613 while the impact was greater in the south part of Shandong Province, and the junction of
614 Henan and Jiangsu Provinces in 2019. For construction dust, the main potential impact areas
615 for 2011-2012 were Beijing, Tianjin, and the western part of Shandong Province, and the
616 southeastern part of Hebei Province, Shanghai, and the eastern part of Hubei Province in
617 2016, while the central and western parts of Shandong Province, the junction of Henan and



618 Shandong Provinces, and the central and southern parts of Anhui Province were the main
619 impact areas in 2019. For sea salt and ship emissions, the potential impact areas for 2011-
620 2012 were mainly located in coastal areas of Jiangsu and Shanghai, which were closely
621 related to the impacts of ship emissions from ports and sea salt in these cities. The Yellow Sea
622 was the main impact area in 2016 and 2019, and the impact areas in 2019 moved to the south.
623 Bie et al. (2021) also analyzed the potential impact areas of ship emissions in Qingdao Port
624 from 2018 to 2019 using the PSCF method, and found that they were mainly located in the
625 Bohai Bay, Yellow Sea, and Yangtze River Delta. Overall, from 2011-2012 to 2019, the
626 potential impact areas of different emission sources in Qingdao have changed markedly. In
627 2019, the potential impact areas for most of the emission sources were mainly located in
628 Shandong Province and along the border areas between the western or southwest parts of
629 Shandong and other provinces, while sea salt and ship emissions were mainly affected by
630 transport on the Yellow Sea.

631

632 **4 Conclusions**

633 A machine learning-based meteorological normalization and a dispersion normalization-
634 based on ventilation coefficient approaches were applied to decouple the meteorological
635 deduced variations in air quality time series and multiple source contributions of a coastal
636 city in northern China (Qingdao), respectively. The concentrations of air pollutants other than
637 ozone in Qingdao decreased substantially and the air quality improved continuously after the
638 “CAAP” period, indicating that the control strategies of air pollution in Qingdao over the
639 years have been proper. The largest emission reduction sections were likely from coal
640 combustions and industrial emissions from 2011-2012 to 2019, and the decrease of steel-
641 related smelting after 2016 due to the relocation of iron and steel enterprises. The
642 contribution of dust in Qingdao decreased remarkably after the “CAAP”, but the impact was
643 still outstanding until 2019. Vehicle emissions were increased in importance, as opposed to
644 the other primary sources. Qingdao risks increased emissions from the increased vehicular
645 population and ozone pollution that facilitate secondary particles formation in the future. In
646 addition, the influence of ship emissions should be gradually reduced. The control of motor-
647 vehicles and dust should be the focus of pollution source control in Qingdao in the future,



while that of coal combustion and industrial sources cannot be ignored. In addition, the potential impact areas of different emission sources in Qingdao have changed markedly from 2011-2012 to 2019. The potential impact areas for most of emission sources were mainly located in Shandong and the border areas between western or southwest Shandong and other provinces in 2019, while sea salt and ship emissions were mainly affected from the transport of the Yellow Sea.

Author contributions

Baoshuang Liu: Data curation, Writing – original draft, Yanyang Wang: Data curation and Investigation, He Meng: Data collection, Qili, Dai: Supervision and Review, Liuli Diao: Data curation, Jianhui Wu: Supervision, Laiyuan Shi: Supervision, Jing Wang: Supervision, Yufen Zhang: Supervision – review & editing, Yinchang Feng: Supervision – review & editing.

Competing interests

The authors declare no competing financial interests.

Acknowledgements

The authors are grateful to the Qingdao Eco-environment Monitoring Center of Shandong Province for collection of particulate matter samples in this study.

Financial support

This study was financially supported by the China Postdoctoral Science Foundation (No. 2019M660986), the Tianjin Science and Technology Plan Project (No. PTZWHZ00120) and the Fundamental Research Funds for the Central Universities: Nankai University (No. 63211074).

References

- Alexander, B., Sherwen, T., Holmes, C. D., Fisher, J. A., Chen, Q., Evans, M. J., and Kasibhatla, P.: Global inorganic nitrate production mechanisms: comparison of a global model with nitrate isotope observations, *Atmos. Chem. Phys.*, 20, 3859-3877, <https://doi.org/10.5194/acp-2019-422>, 2020.
- Begum, B. A., Biswas, S. K., and Hopke, P. K.: Key issues in controlling air pollutants in Dhaka, Bangladesh, *Atmos Environ.*, 45, 7705-7713, <https://doi.org/10.1016/j.atmosenv.2010.10.022>, 2011.
- Beloconi, A., Probst-Hensch, N. M., and Vounatsou, P.: Spatio-temporal modelling of changes in air pollution exposure associated to the COVID-19 lockdown measures across Europe, *Sci Total Environ.*, 787, 147607, <https://doi.org/10.1016/j.scitotenv.2021.147607>, 2021.
- Bi, X. H., Dai, Q. L., Wu, J. H., Zhang, Q., Zhang, W. H., Luo, R. X., Cheng, Y., Zhang, J. Y., Wang, L., Yu,



- 681 Z. J., Zhang, Y. F., Tian, Y. Z., and Feng, Y. C.: Characteristics of the main primary source profiles of
 682 particulate matter across China from 1987 to 2017, *Atmos Chem Phys.*, 19, 3223–3243,
 683 <https://doi.org/10.5194/acp-19-3223-2019>, 2019.
- 684 Bie, S. J., Yang, L. X., Zhang, Y., Huang, Q., Li, J. S., Zhao, T., Zhang, X. F., Wang, P. C., and Wang, W.
 685 X.: 2021. Source appointment of PM_{2.5} in Qingdao Port, East of China, *Sci Total Environ.*, 755,
 686 142456, <https://doi.org/10.1016/j.scitotenv.2020.142456>, 2021.
- 687 Bove, M. C., Brotto, P., Calzolari, G., Cassola, F., Cavalli, F., Fermo, P., Hjorth, J., Massabò, D., Nava,
 688 S., Piazzalunga, A., Schembari, C., and Prati, P.: PM₁₀ source apportionment applying PMF and
 689 chemical tracer analysis to ship-borne measurements in the Western Mediterranean, *Atmos Environ.*,
 690 125, 140–151, <https://doi.org/10.1016/j.atmosenv.2015.11.009>, 2016.
- 691 Brown, S. G., Eberly, S., Paatero, P., and Norris, G. A.: Methods for estimating uncertainty in PMF
 692 solutions: Examples with ambient air and water quality data and guidance on reporting PMF results,
 693 *Sci Total Environ.*, 518, 626–635, <https://doi.org/10.1016/j.scitotenv.2015.01.022>, 2015.
- 694 Chen, Y., Zhang, S. M., Peng, C., Shi, G. M., Tian, M., Huang, R. J., Guo, D. M., Wang, H. B., Yao, X. J.,
 695 Yang, F. M.: Impact of the COVID-19 pandemic and control measures on air quality and aerosol light
 696 absorption in Southwestern China, *Sci Total Environ.*, 749, 141419,
 697 <https://doi.org/10.1016/j.scitotenv.2020.141419>, 2020a.
- 698 Chen, X., Wang, H., Lu, K., Li, C., Zhai, T., Tan, Z., Ma, X., Yang, X., Liu, Y., Chen, S., Dong, H., Li, X.,
 699 Wu, Z., Hu, M., Zeng, L., and Zhang, Y.: Field Determination of Nitrate Formation Pathway in Winter
 700 Beijing, *Environ. Sci. Technol.*, 54, 9243–9253, <https://doi.org/10.1021/acs.est.0c00972>, 2020b .
- 701 Cheng, N. L., Cheng, B. F., Li, S. S., and Ning, T. Z.: Effects of meteorology and emission reduction
 702 measures on air pollution in Beijing during heating seasons, *Atmos Pollut Res.*, 10, 971–979,
 703 <https://doi.org/10.1016/j.apr.2019.01.005>, 2019.
- 704 Choi, J. -K., Heo, J. -B., Ban, S. -J., Yi, S. -M., and Zoh, K. -D.: Source apportionment of PM_{2.5} at the
 705 coastal area in Korea, *Sci Total Environ.*, 447, 370–380,
 706 <https://doi.org/10.1016/j.scitotenv.2012.12.047>, 2013.
- 707 Collivignarelli, M. C., De Rose, C., Abbà, A., Baldi, M., Bertanza, G., Pedrazzani, R., Sorlini, S., and
 708 Carnevale Miino, M.: Analysis of lockdown for COVID-19 impact on NO₂ in London, Milan and
 709 Paris: What lesson can be learnt? *Process Safety and Environmental Protection.*, 146, 952–960
 710 <https://doi.org/10.1016/j.psep.2020.12.029>, 2021.
- 711 Chu, B. W., Zhang, S. P., Liu, J., Ma, Q. X., and He, H.: Significant concurrent decrease in PM_{2.5} and NO₂
 712 concentrations in China during COVID-19 epidemic, *J. Environ. Sci.*, 99, 346–353,
 713 <https://doi.org/10.1016/j.jes.2020.06.031>, 2021.
- 714 Carslaw, D. C.: Worldmet: Import Surface Meteorological Data from NOAA Integrated Surface Database
 715 (ISD), available at: <http://github.com/davidcarslaw/> (last access: 5 September 2018), 2017.
- 716 Cohen, A. J., Brauer, M., Burnett, R., Anderson, H. R., Frostad, J., Estep, K., Balakrishnan, K., Brunekreef,
 717 B., Dandona, L., Dandona, R., Feigin, V., Freedman, G., Hubbell, B., Jobling, A., Kan, H., Knibbs,
 718 L., Liu, Y., Martin, R., Morawska, L., Pope, C. A., Shin, H., Straif, K., Shaddick, G., Thomas, M., van
 719 Dingenen, R., van Donkelaar, A., Vos, T., Murray, C. J. L., and Forouzanfar, M. H.: Estimates and 25-
 720 year trends of the global burden of disease attributable to ambient air pollution: an analysis of data
 721 from the Global Burden of Diseases Study 2015, *The Lancet.*, 389, 1907–1918,
 722 [https://doi.org/10.1016/S0140-6736\(17\)30505-6](https://doi.org/10.1016/S0140-6736(17)30505-6), 2017.
- 723 Cucciniello, R., Raia, L., and Vasca, E.: Air quality evaluation during COVID-19 in Southern Italy: the
 724 case study of Avellino city, *Environ Res.*, 203, 111803, <https://doi.org/10.1016/j.envres.2021.111803>,



- 2022.
- Dai, Q. L., Liu, B. S., Bi, X. H., Wu, J. H., Liang, D. N., Zhang, Y. F., Feng, Y. C., and Hopke, P. K.: Dispersion Normalized PMF Provides Insights into the Significant Changes in Source Contributions to PM_{2.5} after the COVID-19 Outbreak, *Environ. Sci. Technol.*, 54, 9917-9927, <https://doi.org/10.1021/acs.est.0c02776>, 2020.
- Dai, Q., Hou, L., Liu, B., Zhang, Y., Song, C., Shi, Z., Hopke, P. K., and Feng, Y.: Spring Festival and COVID-19 Lockdown: Disentangling PM Sources in Major Chinese Cities, *Geophys. Res. Lett.*, 48, 11, <https://doi.org/10.1029/2021GL093403>, 2021.
- Dai, Q., Ding, J., Hou, L., Li, L., Cai, Z., Liu, B., Song, C., Bi, X., Wu, J., Zhang, Y., Feng, Y., and Hopke, P. K.: Haze episodes before and during the COVID-19 shutdown in Tianjin, China: Contribution of fireworks and residential burning, *Environ. Pollut.*, 286, 117252, <https://doi.org/10.1016/j.envpol.2021.117252>, 2021.
- Ding, J., Dai, Q. L., Li, Y. F., Han, S. Q., Zhang, Y. F., and Feng, Y. C.: Impact of meteorological condition changes on air quality and particulate chemical composition during the COVID-19 lockdown, *J. Environ. Sci.*, 109, 45-56, <https://doi.org/10.1016/j.jes.2021.02.022>, 2021.
- Esmailirad, S., Lai, A., Abbaszade, G., Schnelle-Kreis, J., Zimmermann, R., Uzu, G., Daellenbach, K., Canonaco, F., Hassankhany, H., Arhami, M., Baltensperger, U., Prévôt, A. S. H., Schauer, J. J., Jaffrezo, J. -L., Hosseini, V., and El Haddad, I.: Source apportionment of fine particulate matter in a Middle Eastern Metropolis, Tehran-Iran, using PMF with organic and inorganic markers, *Sci. Total Environ.*, 705, 135330, <https://doi.org/10.1016/j.scitotenv.2019.135330>, 2020.
- Fu, X., Wang, T., Gao, J., Wang, P., Liu, Y. M., Wang, S. X., Zhao, B., and Xue, L. K.: Persistent Heavy Winter Nitrate Pollution Driven by Increased Photochemical Oxidants in Northern China, *Environ. Sci. Technol.*, 54, 3881-3889, <https://doi.org/10.1021/acs.est.9b07248>, 2020.
- Gao, J., Peng, X., Chen, G., Xu, J., Shi, G. L., Zhang, Y. C., and Feng, Y. C.: Insights into the chemical characterization and sources of PM_{2.5} in Beijing at a 1-h time resolution, *Sci. Total Environ.*, 542, 162-171, <https://doi.org/10.1016/j.scitotenv.2015.10.082>, 2016.
- Gao, Y., Shan, H. Y., Zhang, S. Q., Sheng, L. F., Li, J. P., Zhang, J. X., Ma, M. C., Meng, H., Luo, K., Gao, H. W., and Yao, X. H.: Characteristics and sources of PM_{2.5} with focus on two severe pollution events in a coastal city of Qingdao, China, *Chemosphere*, 247, 125861, <https://doi.org/10.1016/j.chemosphere.2020.125861>, 2020.
- Grange, S. K., Carslaw, D. C., Lewis, A. C., Boleti, E., and Hueglin, C.: Random forest meteorological normalization models for Swiss PM₁₀ trend analysis, *Atmos Chem Phys.*, 18, 6223-6239, <https://doi.org/10.5194/acp-18-6223-2018>, 2018.
- Grange, S. K., and Carslaw, D. C.: Using meteorological normalization to detect interventions in air quality time series, *Sci. Total Environ.*, 653, 578-588, <https://doi.org/10.1016/j.scitotenv.2018.10.344>, 2019.
- Gulia, S., Mittal, A., and Khare, M.: Quantitative evaluation of source interventions for urban air quality improvement - A case study of Delhi city, *Atmos Pollut Res.*, 9, 577-583, <https://doi.org/10.1016/j.apr.2017.12.003>, 2018.
- He, G. J., Pan, Y. H., and Tanaka, T.: The short-term impacts of COVID-19 lockdown on urban air pollution in China, *Nat. Sustainability*, 3, 1005-1011, <https://doi.org/10.1038/s41893-020-0581-y>, 2020.
- Huang, H. Y., Liu, B. S., Li, S., Choe, T. -H., Dai, Q. L., Gu, Y., Diao, L. L., Zhang, S. F., Bi, X. H., Luo, Z. W., Lu, M. M., Zhang, Y. F., and Feng, Y. C.: An estimation method for regional transport contributions from emission sources based on a high-mountain site: a case study in Zhumadian, China.



- 769 Atmos. Environ., 263, 118664, <https://doi.org/10.1016/j.atmosenv.2021.118664>, 2021.
- 770 Huang, J., Pan, X. C., Guo, X. B., and Li, G. X.: 2018. Health impact of China's Air Pollution Prevention
 771 and Control Action Plan: an analysis of national air quality monitoring and mortality data, *The Lancet*
 772 *Planetary Health.*, 2, e313-e323, [https://doi.org/10.1016/S2542-5196\(18\)30141-4](https://doi.org/10.1016/S2542-5196(18)30141-4), 2018.
- 773 Huang, R. J., Zhang, Y. L., Bozzetti, C., Ho, K. F., Cao, J. J., Han, Y. M., Daellenbach, K. R., Slowik, J.
 774 G., Platt, S. M., Canonaco, F., Zotter, P., Wolf, R., Pieber, S. M., Bruns, E. A., Crippa, M., Ciarelli,
 775 G., Piazzalunga, A., Schwikowski, M., Abbaszade, G., Schnelle-Kreis, J., Zimmermann, R., An, Z.
 776 S., Szidat, S., Baltensperger, U., El Haddad, I., and Prevot, A. S. H.: High secondary aerosol
 777 contribution to particulate pollution during haze events in China, *Nature*, 514, 218-222,
 778 <https://doi.org/10.1038/nature13774>, 2014.
- 779 Huang, X. J., Liu, Z. R., Liu, J. Y., Hu, B., Wen, T. X., Tang, G. Q., Zhang, J. K., Wu, F. K., Ji, D. S., Wang,
 780 L. L., and Wang, Y. S.: Chemical characterization and source identification of PM_{2.5} at multiple sites
 781 in the Beijing-Tianjin-Hebei region, China, *Atmos Chem Phys.*, 17, 12941-12962, 10.5194/acp-17-
 782 12941-2017, 2017.
- 783 Hopke, P. K., Dai, Q., Li, L., and Feng, Y.: Global review of recent source apportionments for airborne
 784 particulate matter, *Sci. Total Environ.*, 740, 140091, <https://doi.org/10.1016/j.scitotenv.2020.140091>,
 785 2020.
- 786 Hong, Y. W., Xu, X. B., Liao, D., Zheng, R. H., Ji, X. T., Chen, Y. T., Xu, L. L., Li, M. R., Wang, H., Xiao,
 787 H., Choi, S. D., Chen, J. S.: Source apportionment of PM_{2.5} and sulfate formation during the COVID-
 788 19 lockdown in a coastal city of southeast China, *Environ. Pollut.*, 286, 117577,
 789 <https://doi.org/10.1016/j.envpol.2021.117577>, 2021.
- 790 Iyer, U. S., and Raj, P. E.: Ventilation coefficient trends in the recent decades over four major Indian
 791 metropolitan cities, *J. Earth Syst. Sci.*, 122, 537-549, <https://doi.org/10.1007/s12040-013-0270-6>,
 792 2013.
- 793 Jain, S., Sharma, S. K., Mandal, T. K., and Saxena, M.: Source apportionment of PM₁₀ in Delhi, India
 794 using PCA/APCS, UNMIX and PMF, *Particuology*, 37, 107-118,
 795 <https://doi.org/10.1016/j.partic.2017.05.009>, 2018.
- 796 Jain, S., Sharma, S. K., Vijayan, N., and Mandal, T. K.: Seasonal characteristics of aerosols (PM_{2.5} and
 797 PM₁₀) and their source apportionment using PMF: A four year study over Delhi, India, *Environ Pollut.*,
 798 262, 114337, <https://doi.org/10.1016/j.envpol.2020.114337>, 2020.
- 799 Jiang, X., Li, G. L., and Fu, W.: Government environmental governance, structural adjustment and air
 800 quality: A quasi-natural experiment based on the Three-year Action Plan to Win the Blue Sky Defense
 801 War, *J. Environ. Manage.*, 277, 111470, <https://doi.org/10.1016/j.jenvman.2020.111470>, 2021.
- 802 Joshi, P., Ghosh, S., Dey, S., Dixit, K., Choudhary, R. K., Salve, H. R., and Balakrishnan, K.: Impact of
 803 acute exposure to ambient PM_{2.5} on non-trauma all-cause mortality in the megacity Delhi, *Atmos*
 804 *Environ.* 259, 118548, <https://doi.org/10.1016/j.atmosenv.2021.118548>, 2021.
- 805 Kleinman, M. T., Kneip, T. J., and Eisenbud, M.: Seasonal patterns of airborne particulate concentrations
 806 in New York City, *Atmos. Environ.* (1967), 10, 9-11, [https://doi.org/10.1016/0004-6981\(76\)90252-3](https://doi.org/10.1016/0004-6981(76)90252-3),
 807 1976.
- 808 Kuo, S. -C., Hsieh, L. -Y., Tsai, C. -H., and Tsai, Y. I.: Characterization of PM_{2.5} fugitive metal in the
 809 workplaces and the surrounding environment of a secondary aluminum smelter, *Atmos. Environ.*, 41,
 810 6884-6900, <https://doi.org/10.1016/j.atmosenv.2007.04.038>, 2007.
- 811 Le, T. H., Wang, Y., Liu, L., Yang, J. N., Yung, Y. L., Li, G. H., and Seinfeld, J. H.: Unexpected air
 812 pollution with marked emission reductions during the COVID-19 outbreak in China, *Science*, 369,



- 702, <https://doi.org/10.1126/science.abb7431>, 2020.
- Li, L. Y., Yan, D. Y., Xu, S. H., Huang, M. L., Wang, X. X., and Xie, S. D.: Characteristics and source distribution of air pollution in winter in Qingdao, eastern China. *Environ Pollut.* 224, 44-53, <https://doi.org/10.1016/j.envpol.2016.12.037>, 2017.
- Li, W. J., Shao, L. Y., Wang, W. H., Li, H., Wang, X. M., Li, Y. W., Li, W. J., Jones, T., and Zhang, D. Z.: Air quality improvement in response to intensified control strategies in Beijing during 2013–2019, *Sci. Total Environ.*, 744, 140776, <https://doi.org/10.1016/j.scitotenv.2020.140776>, 2020.
- Li, Y., Miao, Y. C., Che, H. Z., and Liu, S. H.: On the heavy aerosol pollution and its meteorological dependence in Shandong province, China, *Atmos Res.*, 256, 105572, <https://doi.org/10.1016/j.atmosres.2021.105572>, 2021a.
- Li, Y., Xu, H. X., Tang, K. Y., Lau, A. K. H., Fung, J. C. H., and Zhang, X. G.: An ensemble assessment of the effectiveness of vehicular emission control programs for air quality improvement in Hong Kong, *Atmos Environ.*, 262, 118571, <https://doi.org/10.1016/j.atmosenv.2021.118571>, 2021b.
- Liang, X., Li, S., Zhang, S. Y., Huang, H., and Chen, S. X.: PM_{2.5} data reliability, consistency, and air quality assessment in five Chinese cities, *J. Geophys. Res. -Atmos.*, 121, 10220-10236, [10.1002/2016JD024877](https://doi.org/10.1002/2016JD024877), 2016.
- Liu, B. S., Li, Y. F., Wang, L., Bi, X. H., Dong, H. Y., Sun, X. Y., Xiao, Z. M., Zhang, Y. F., and Feng, Y. C.: Source directional apportionment of ambient PM_{2.5} in urban and industrial sites at a megacity in China, *Atmos Res.*, 235, 104764, <https://doi.org/10.1016/j.atmosres.2019.104764>, 2020.
- Liu, B. S., Wu, J. H., Wang, J., Shi, L. Y., Meng, H., Dai, Q. L., Wang, J., Song, C. B., Zhang, Y. F., Feng, Y. C., and Hopke, P. K.: Chemical characteristics and sources of ambient PM_{2.5} in a harbor area: Quantification of health risks to workers from source-specific selected toxic elements, *Environ Pollut.*, 268, 115926, <https://doi.org/10.1016/j.envpol.2020.115926>, 2021a.
- Liu, M., Saari, R. K., Zhou, G. X., Li, J., Han, L., and Liu, X. N.: Recent trends in premature mortality and health disparities attributable to ambient PM_{2.5} exposure in China: 2005–2017, *Environ Pollut.*, 279, 116882, <https://doi.org/10.1016/j.envpol.2021.116882>, 2021b.
- Liu, W. J., Xu, Y. S., Liu, W. X., Liu, Q. Y., Yu, S. Y., Liu, Y., Wang, X., and Tao, S.: Oxidative potential of ambient PM_{2.5} in the coastal cities of the Bohai Sea, northern China: Seasonal variation and source apportionment, *Environ Pollut.*, 236, 514-528, <https://doi.org/10.1016/j.envpol.2018.01.116>, 2018.
- Liu F., Beirle S., Zhang Q., van der A. R. J., Zheng B., Tong D., and He K.: NO_x emission trends over Chinese cities estimated from OMI observations during 2005 to 2015, *Atmos. Chem. Phys.*, 17, 9261-9275, <https://doi.org/10.5194/acp-17-9261-2017>, 2017.
- Lyu, X. P., Zeng, L. W., Guo, H., Simpson, I. J., Ling, Z. H., Wang, Y., Murray, F., Louie, P. K., Saunders, S. M., Lam, S. H. M., and Blake, D. R.: Evaluation of the effectiveness of air pollution control measures in Hong Kong, *Environ Pollut.*, 220, 87-94, <https://doi.org/10.1016/j.envpol.2016.09.025>, 2017.
- Ma, X. W., Li, C. D., Dong, X. Y., and Liao, H.: Empirical analysis on the effectiveness of air quality control measures during mega events: Evidence from Beijing, China, *J. Clean Prod.*, 271, 122536, <https://doi.org/10.1016/j.jclepro.2020.122536>, 2020.
- Manousakas, M., Papaefthymiou, H., Diapoulis, E., Migliori, A., Karydas, A. G., Bogdanovic-Radovic, I., and Eleftheriadis, K.: Assessment of PM_{2.5} sources and their corresponding level of uncertainty in a coastal urban area using EPA PMF 5.0 enhanced diagnostics, *Sci. Total Environ.*, 574, 155-164, <https://doi.org/10.1016/j.scitotenv.2016.09.047>, 2017.
- Masiol, M., Squizzato, S., Rich, D. Q., and Hopke, P. K.: Long-term trends (2005–2016) of source



- 857 apportioned PM_{2.5} across New York State, *Atmos Environ.*, 201, 110-120,
 858 <https://doi.org/10.1016/j.atmosenv.2018.12.038>, 2019.
- 859 Meng, Z. Y., Ding, G. A., Xu, X. B., Xu, X. D., Yu, H. Q., and Wang, S. F.: Vertical distributions of SO₂
 860 and NO₂ in the lower atmosphere in Beijing urban areas, China, *Sci. Total Environ.*, 390, 456-465,
 861 <https://doi.org/10.1016/j.scitotenv.2007.10.012>, 2008.
- 862 Munir, S., Chen, H. B., and Ropkins, K.: Quantifying temporal trends in ground level ozone concentration
 863 in the UK, *Sci. Total Environ.*, 458-460, 217-227, <https://doi.org/10.1016/j.scitotenv.2013.04.045>,
 864 2013.
- 865 Nirel, R., and Dayan, U.: On the ratio of sulfur dioxide to nitrogen oxides as an indicator of air pollution
 866 sources, *J. Appl. Meteorol.*, 40, 1209-1222 [10.1175/1520-0450\(2001\)040<1209:OTROSD>2.0.CO;2](https://doi.org/10.1175/1520-0450(2001)040<1209:OTROSD>2.0.CO;2),
 867 2001.
- 868 Paatero, P., and Tapper, U.: Positive matrix factorization: A non-negative factor model with optimal
 869 utilization of error estimates of data values. *Environmetrics*, 5, 111-126,
 870 <https://doi.org/10.1002/env.3170050203>, 1994.
- 871 Police, S., Sahu, S. K., and Pandit, G. G.: Chemical characterization of atmospheric particulate matter and
 872 their source apportionment at an emerging industrial coastal city, Visakhapatnam, India, *Atmos. Pollut.*
 873 *Res.*, 7, 725-733, <https://doi.org/10.1016/j.apr.2016.03.007>, 2016.
- 874 Pugliese, S. C., Murphy, J. G., Geddes, J. A., and Wang, J. M.: The impacts of precursor reduction and
 875 meteorology on ground-level ozone in the Greater Toronto Area, *Atmos. Chem. Phys.*, 14, 8197-8207,
 876 <https://doi.org/10.5194/acp-14-8197-2014>, 2014.
- 877 Qi, L., Zhang, Y. F., Ma, Y. H., Chen, M. D., Ge, X. L., Ma, Y., Zheng, J., Wang, Z., and Li, S.Z.: Source
 878 identification of trace elements in the atmosphere during the second Asian Youth Games in Nanjing,
 879 China: Influence of control measures on air quality, *Atmos. Pollut. Res.*, 7, 547-556,
 880 <https://doi.org/10.1016/j.apr.2016.01.003>, 2016.
- 881 Querol, X., Viana, M., Alastuey, A., Amato, F., Moreno, T., Castillo, S., Pey, J., de la Rosa, J., Sánchez de
 882 la Campa, A., Artíñano, B., Salvador, P., García Dos Santos, S., Fernández-Patier, R., Moreno-Grau,
 883 S., Negral, L., Minguillón, M. C., Monfort, E., Gil, J. I., Inza, A., Ortega, L. A., Santamaría, J. M., and
 884 Zabalza, J.: Source origin of trace elements in PM from regional background, urban and industrial
 885 sites of Spain, *Atmos Environ.*, 41, 7219-7231, <https://doi.org/10.1016/j.atmosenv.2007.05.022>, 2007.
- 886 Ryou, H. G., Heo, J., and Kim, S. Y.: Source apportionment of PM₁₀ and PM_{2.5} air pollution, and possible
 887 impacts of study characteristics in South Korea, *Environ Pollut.*, 240, 963-972,
 888 <https://doi.org/10.1016/j.envpol.2018.03.066>, 2018.
- 889 Sen, P. K.: Estimates of the Regression Coefficient Based on Kendall's Tau AU – Sen, Pranab Kumar, J.
 890 *Am. Stat. Assoc.*, 63, 1379–1389, <https://doi.org/10.1080/01621459.1968.10480934>, 1968.
- 891 Schleicher, N., Norra, S., Chen, Y., Chai, F., and Wang, S.: Efficiency of mitigation measures to reduce
 892 particulate air pollution—A case study during the Olympic Summer Games 2008 in Beijing, China,
 893 *Sci. Total Environ.*, 427-428, 146-158, <https://doi.org/10.1016/j.scitotenv.2012.04.004>, 2012.
- 894 Shi, Z. B., Song, C. B., Liu, B. W., Lu, G. D., Xu, J. S., Vu, T. V., Elliott, R. J. R., Li, W. J., Bloss, W. J.,
 895 and Harrison, R.M.: Abrupt but smaller than expected changes in surface air quality attributable to
 896 COVID-19 lockdowns, *Sci Adv.*, 7, eabd6696, <https://doi.org/10.1126/sciadv.abd6696>, 2021.
- 897 Sofowote, U. M., Healy, R. M., Su, Y., Deboz, J., Noble, M., Munoz, A., Jeong, C. H., Wang, J. M., Hilker,
 898 N., Evans, G. J., Brook, J. R., Lu, G., and Hopke, P. K.: Sources, variability and parameterizations of
 899 intra-city factors obtained from dispersion-normalized multi-time resolution factor analyses of PM_{2.5}
 900 in an urban environment, *Sci. Total Environ.*, 761, 143225,



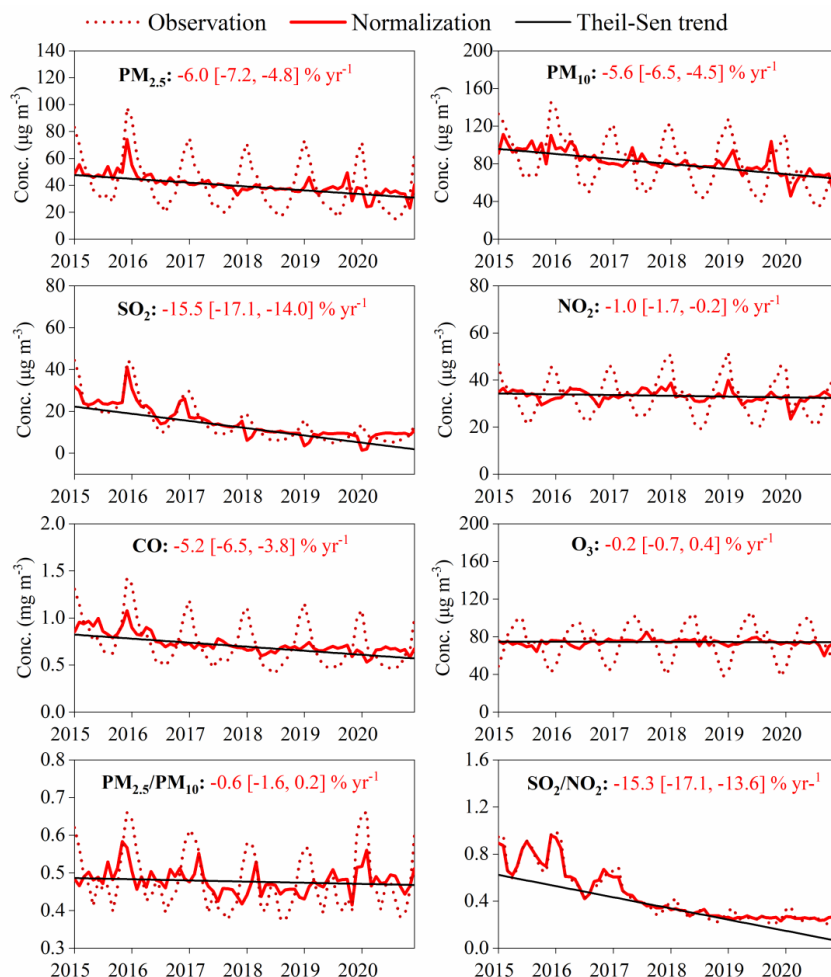
- 901 <https://doi.org/10.1016/j.scitotenv.2020.143225>, 2021.
- 902 Song, L. L., Dai, Q. L., Feng, Y. C., and Hopke, P. K.: Estimating uncertainties of source contributions to
 903 PM_{2.5} using moving window evolving dispersion normalized PMF, *Environ Pollut.*, 286, 117576,
 904 <https://doi.org/10.1016/j.envpol.2021.117576>, 2021.
- 905 Sujatha, P., Mahalakshmi, D. V., Ramiz, A., Rao, P. V. N., and Naidu, C.V.: Ventilation coefficient and
 906 boundary layer height impact on urban air quality, *Cogent Environ. Sci.*, 2, 1125284
 907 <https://doi.org/10.1080/23311843.2015.1125284>, 2016.
- 908 Tao, J., Gao, J., Zhang, L., Zhang, R., Che, H., Zhang, Z., Lin, Z., Jing, J., Cao, J., and Hsu, S. C.: PM_{2.5}
 909 pollution in a megacity of southwest China: source apportionment and implication, *Atmos. Chem.*
 910 *Phys.*, 14, 8679-8699, <https://doi.org/10.5194/acp-14-8679-2014>, 2014.
- 911 Tian, Y. Z., Wang, J., Peng, X., Shi, G. L., and Feng, Y.C.: Estimation of the direct and indirect impacts of
 912 fireworks on the physicochemical characteristics of atmospheric PM₁₀ and PM_{2.5}, *Atmos. Chem. Phys.*,
 913 14, 9469-9479, <https://doi.org/10.5194/acp-14-9469-2014>, 2014.
- 914 Tsai, P. J., Young, L. H., Hwang, B. F., Lin, M. Y., Chen, Y. C., and Hsu, H.T.: Source and health risk
 915 apportionment for PM_{2.5} collected in Sha-Lu area, Taiwan, *Atmos. Pollut. Res.*, 11, 851-858,
 916 <https://doi.org/10.1016/j.apr.2020.01.013>, 2020.
- 917 Tsai, D. H., Wang, J. L., Chuang, K. J., and Chan, C. C.: Traffic-related air pollution and cardiovascular
 918 mortality in central Taiwan, *Sci. Total Environ.*, 408, 1818-1823,
 919 <https://doi.org/10.1016/j.scitotenv.2010.01.044>, 2010.
- 920 Vodonos, A., and Schwartz, J.: Estimation of excess mortality due to long-term exposure to PM_{2.5} in
 921 continental United States using a high-spatiotemporal resolution model, *Environ. Res.*, 196, 110904,
 922 <https://doi.org/10.1016/j.envres.2021.110904>, 2021.
- 923 Vu, T. V., Shi, Z. B., Cheng, J., Zhang, Q., He, K. B., Wang, S. X., and Harrison, R.M.: Assessing the
 924 impact of clean air action on air quality trends in Beijing using a machine learning technique, *Atmos.*
 925 *Chem. Phys.*, 19, 11303-11314, <https://doi.org/10.5194/acp-19-11303-2019>, 2019.
- 926 Wang, H. L., Miao, Q., Shen, L. J., Yang, Q., Wu, Y. Z., and Wei, H.: Air pollutant variations in Suzhou
 927 during the 2019 novel coronavirus (COVID-19) lockdown of 2020: High time-resolution
 928 measurements of aerosol chemical compositions and source apportionment, *Environ. Pollut.*, 271,
 929 116298, <https://doi.org/10.1016/j.envpol.2020.116298>, 2021a.
- 930 Wang, S. X., Xing, J., Zhao, B., Jang, C., and Hao, J. M.: Effectiveness of national air pollution control
 931 policies on the air quality in metropolitan areas of China, *J. Environ. Sci.*, 26, 13-22,
 932 [https://doi.org/10.1016/S1001-0742\(13\)60381-2](https://doi.org/10.1016/S1001-0742(13)60381-2), 2014.
- 933 Wang, Y., Xue, Y. F., Tian, H. Z., Gao, J., Chen, Y., Zhu, C. Y., Liu, H. J., Wang, K., Hua, S. B., Liu, S. H.,
 934 and Shao, P. Y.: Effectiveness of temporary control measures for lowering PM_{2.5} pollution in Beijing
 935 and the implications, *Atmos. Environ.*, 157, 75-83, <https://doi.org/10.1016/j.atmosenv.2017.03.017>,
 936 2017.
- 937 Wang, Y. Y., Liu, B. S., Zhang, Y. F., Dai, Q. L., Song, C. B., Duan, L. Q., Guo, L. L., Zhao, J., Xue, Z.
 938 G., Bi, X. H., and Feng, Y. C.: Potential health risks of inhaled toxic elements and risk sources during
 939 different COVID-19 lockdown stages in Linfen, China, *Environ. Pollut.*, 284, 117454,
 940 <https://doi.org/10.1016/j.envpol.2021.117454>, 2021b.
- 941 Xu, H., Xiao, Z. M., Chen, K., Tang, M., Zheng, N. Y., Li, P., Yang, N., Yang, W., and Deng, X. W.: Spatial
 942 and temporal distribution, chemical characteristics, and sources of ambient particulate matter in the
 943 Beijing-Tianjin-Hebei region, *Sci. Total Environ.*, 658, 280-293,
 944 <https://doi.org/10.1016/j.scitotenv.2018.12.164>, 2019a.



- 945 Xu, L. L., Jiao, L., Hong, Z. Y., Zhang, Y. R., Du, W. J., Wu, X., Chen, Y. T., Deng, J. J., Hong, Y. W., and
 946 Chen, J. S.: Source identification of PM_{2.5} at a port and an adjacent urban site in a coastal city of
 947 China: Impact of ship emissions and port activities, *Sci. Total Environ.*, 634, 1205-1213,
 948 <https://doi.org/10.1016/j.scitotenv.2018.04.087>, 2018.
- 949 Xu, M., Qin, Z. F., Zhang, S. H., and Xie, Y.: Health and economic benefits of clean air policies in China:
 950 A case study for Beijing-Tianjin-Hebei region, *Environ. Pollut.*, 285, 117525,
 951 <https://doi.org/10.1016/j.envpol.2021.117525>, 2021.
- 952 Xu, W., Liu, X. J., Liu, L., Dore, A. J., Tang, A., Lu, L., Wu, Q. H., Zhang, Y. Y., Hao, T. X., Pan, Y.
 953 P., Chen, J. M., and Zhang, F. S.: Impact of emission controls on air quality in Beijing during APEC
 954 2014: Implications from water-soluble ions and carbonaceous aerosol in PM_{2.5} and their precursors,
 955 *Atmos. Environ.*, 210, 241-252, <https://doi.org/10.1016/j.atmosenv.2019.04.050>, 2019b.
- 956 Yin, H., Liu, C., Hu, Q. H., Liu, T., Wang, S., Gao, M., Xu, S. Q., Zhang, C. X., and Su, W. J.: Opposite
 957 impact of emission reduction during the COVID-19 lockdown period on the surface concentrations of
 958 PM_{2.5} and O₃ in Wuhan, China, *Environ Pollut.*, 289, 117899,
 959 <https://doi.org/10.1016/j.envpol.2021.117899>, 2021.
- 960 Yu, M. F., Zhu, Y., Lin, C. J., Wang, S. X., Xing, J., Jang, C., Huang, J. Z., Huang, J. Y., Jin, J. B., and Yu,
 961 L.: Effects of air pollution control measures on air quality improvement in Guangzhou, China, *J.*
 962 *Environ. Manage.*, 244, 127-137, <https://doi.org/10.1016/j.jenvman.2019.05.046>, 2019.
- 963 Zhang, D. Z., and Iwasaka, Y.: Nitrate and sulfate in individual Asian dust-storm particles in Beijing, China
 964 in Spring of 1995 and 1996, *Atmos. Environ.*, 33, 3213-3223, [https://doi.org/10.1016/S1352-](https://doi.org/10.1016/S1352-2310(99)00116-8)
 965 [2310\(99\)00116-8](https://doi.org/10.1016/S1352-2310(99)00116-8), 1999.
- 966 Zhang, D. Z., Shi, G. Y., Iwasaka, Y., Hu, M., and Zang, J. Y.: Anthropogenic Calcium Particles Observed
 967 in Beijing and Qingdao, China, *Water, Air, & Soil Pollution: Focus.*, 5, 261-276,
 968 <https://doi.org/10.1007/s11267-005-0743-y>, 2005.
- 969 Zhang, Q., He, K. B., and Huo, H.: Cleaning China's air. *Nature*. 484, 161-162,
 970 <https://doi.org/10.1038/484161a>, 2012.
- 971 Zhang, Q., Zheng, Y. X., Tong, D., Shao, M., Wang, S. X., Zhang, Y. H., Xu, X. D., Wang, J. N., He,
 972 H., Liu, W. Q., Ding, Y. H., Lei, Y., Li, J. H., Wang, Z. F., Zhang, X. Y., Wang, Y. S., Cheng, J., Liu,
 973 Y., Shi, Q. R., Yan, L., Geng, G. N., Hong, C. P., Li, M., Liu, F., Zheng, B., Cao, J. J., Ding, A. J., Gao,
 974 J., Fu, Q. Y., Huo, J. T., Liu, B. X., Liu, Z. R., Yang, F. M., He, K. B., and Hao, J. M.: Drivers of
 975 improved PM_{2.5} air quality in China from 2013 to 2017, *Proceedings of the National Academy of*
 976 *Sciences*, 116, 24463-24469, <https://doi.org/10.1073/pnas.1907956116>, 2019.
- 977 Zhang, Y., Yang, L. X., Bie, S. J., Zhao, T., Huang, Q., Li, J. S., Wang, P. C., Wang, Y. M., and Wang, W. X.:
 978 Chemical compositions and the impact of sea salt in atmospheric PM₁ and PM_{2.5} in the coastal area,
 979 *Atmos. Res.*, 250, 105323, <https://doi.org/10.1016/j.atmosres.2020.105323>, 2021.
- 980 Zhao, S., Tian, H. Z., Luo, L. N., Liu, H. J., Wu, B. B., Liu, S. H., Bai, X. X., Liu, W., Liu, X. Y., Wu, Y.
 981 M., Lin, S. M., Guo, Z. H., Lv, Y. Q., and Xue, Y. F.: Temporal variation characteristics and source
 982 apportionment of metal elements in PM_{2.5} in urban Beijing during 2018–2019, *Environ. Pollut.*, 268,
 983 115856, <https://doi.org/10.1016/j.envpol.2020.115856>, 2021.
- 984 Zong, Z., Wang, X. P., Tian, C. G., Chen, Y. J., Fu, S. F., Qu, L., Ji, L., Li, J., and Zhang, G.: PMF and
 985 PSCF based source apportionment of PM_{2.5} at a regional background site in North China, *Atmos. Res.*,
 986 203, 207-215, <https://doi.org/10.1016/j.atmosres.2017.12.013>, 2018.



989



990

991 **Figure 1.** Trends of air pollutant concentrations and $\text{PM}_{2.5}/\text{PM}_{10}$ and SO_2/NO_2 from 2015 to
 992 2020. “Observation” represents the observed data, and “Normalization” in represents the
 993 modelled concentrations of air pollutants after weather normalization. The black line shows
 994 the Theil–Sen trend after weather normalization.

995

996

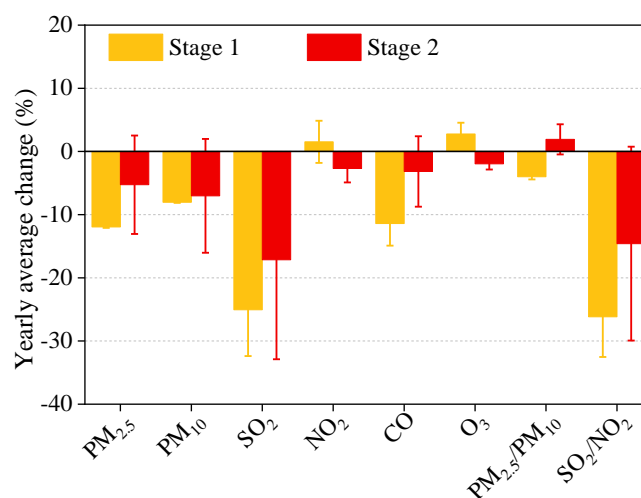


Figure 2. Yearly average change of air pollutants and PM_{2.5}/PM₁₀ and SO₂/NO₂ during different pollution-control stages based on the weather normalized data.

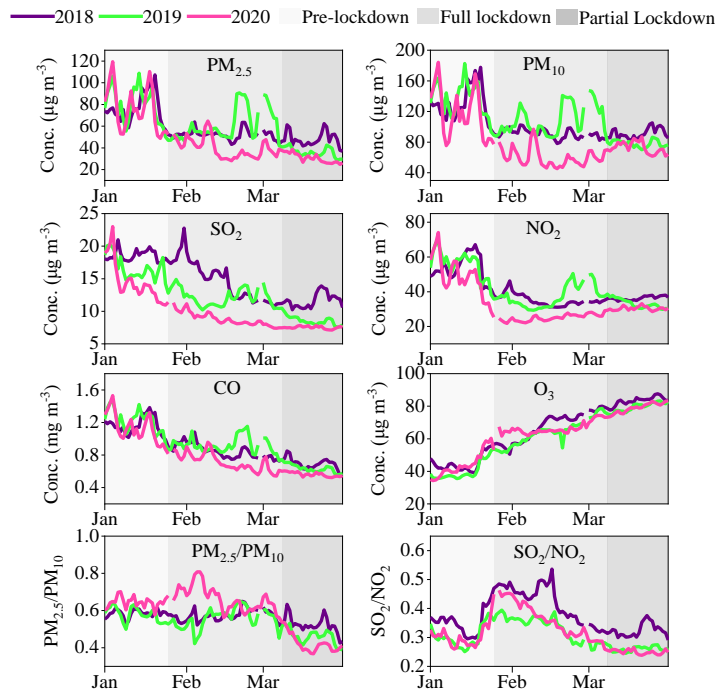


Figure 3. Time series of air pollutants concentrations and PM_{2.5}/PM₁₀ and SO₂/NO₂ during the different stages of COVID-19 lockdown start dates or equivalent in 2020 versus 2018 and 2019 based on the weather normalization data.

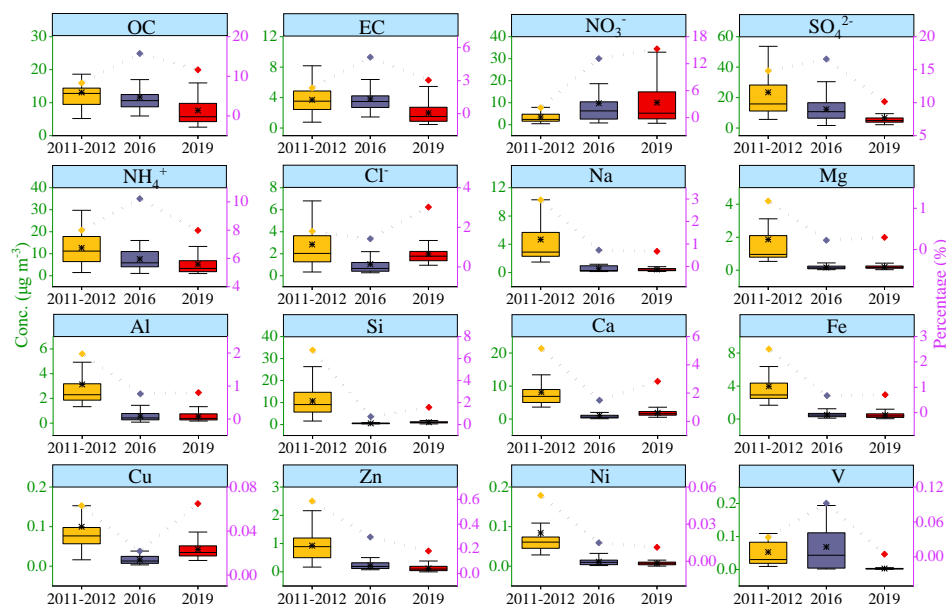


Figure 4. Variations of the average concentrations and percentages of major chemical compositions of PM_{2.5} in 2011-2012, 2016, and 2019. Box charts represent concentrations, and line charts represent percentages.

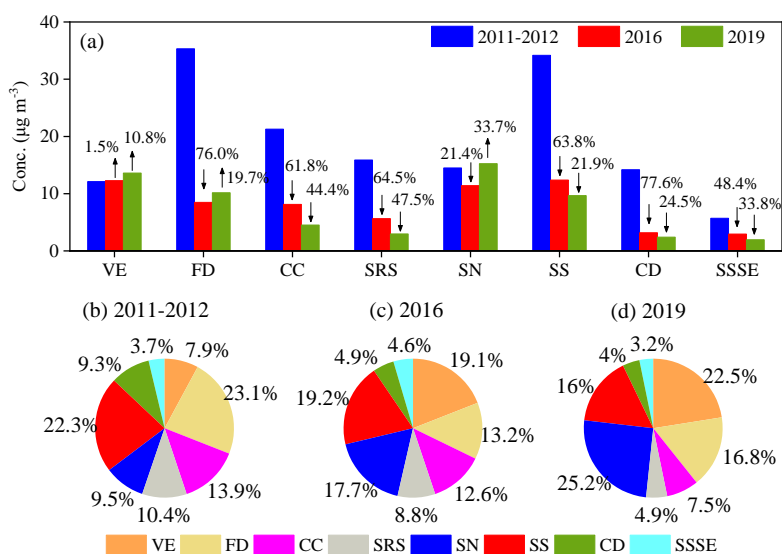


Figure 5. Changes in source contributions for 2011-2012, 2016, and 2019. VE represents vehicle emissions, FD represents fugitive dust, CC represents coal combustion, SRS represents steel-related smelting, SN represents secondary nitrate, SS represents secondary sulphate, CD represents construction dust, and SSSE represents sea salt and ship emissions.

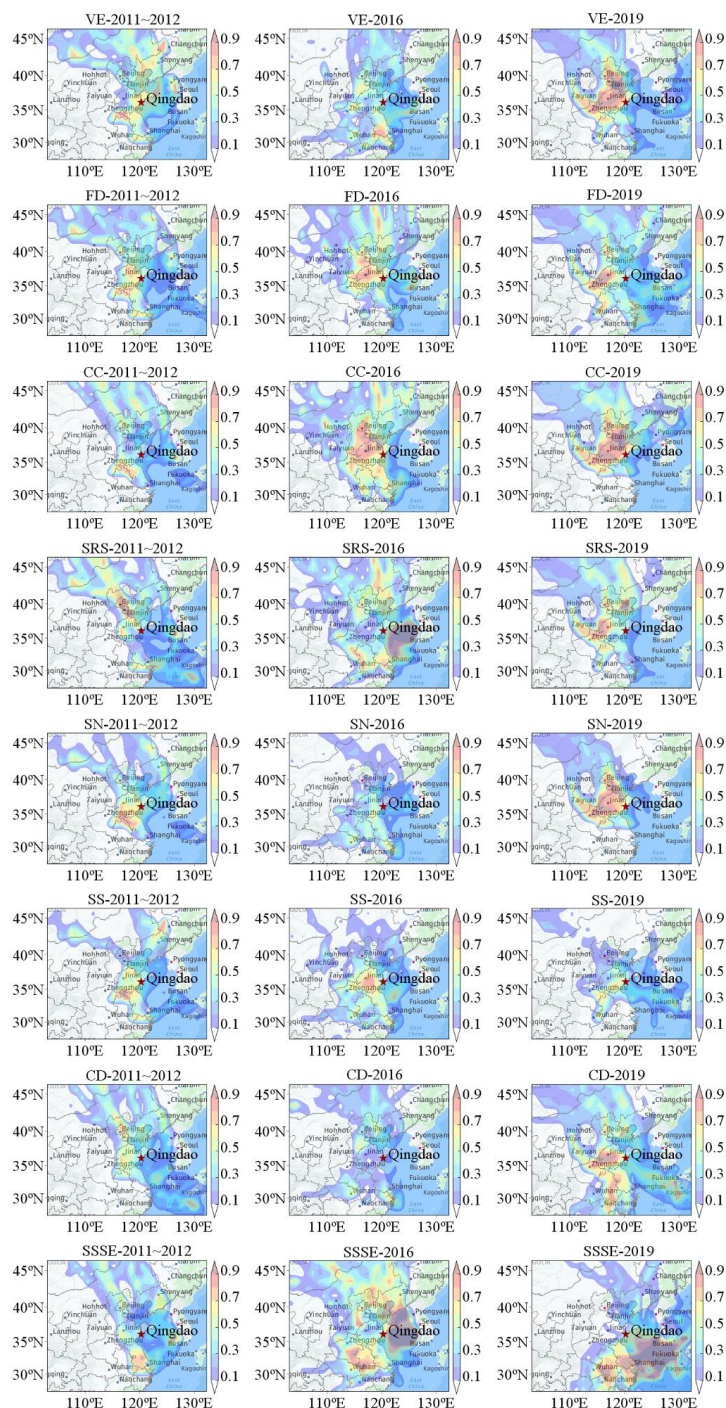


Figure 6. WPSCF plots for various emission sources during different periods (base map from Yahoo Maps). VE represents vehicle emissions, FD represents fugitive dust, CC represents



1020 coal combustion, SRS represents steel-related smelting, SN represents secondary nitrate, SS
1021 represents secondary sulphate, CD represents construction dust, and SSSE represents sea salt
1022 and ship emissions.
1023